


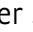




Quorum sensing governs a transmissible *Legionella* subpopulation at the pathogen vacuole periphery

Bianca Striednig¹ , Ulrike Lanner², Selina Niggli^{1,†} , Ana Katic¹, Simone Vormittag¹, Sabrina Brülisauer¹, Ramon Hochstrasser¹, Andres Kaech³, Amanda Welin⁴, Antje Flieger⁵, Urs Ziegler³ , Alexander Schmidt² , Hubert Hilbi^{1,*,†}  & Nicolas Personnic^{1,**,†} 

Abstract

The Gram-negative bacterium *Legionella pneumophila* is the causative agent of Legionnaires' disease and replicates in amoebae and macrophages within a distinct compartment, the *Legionella*-containing vacuole (LCV). The facultative intracellular pathogen switches between a replicative, non-virulent and a non-replicating, virulent/transmissible phase. Here, we show on a single-cell level that at late stages of infection, individual motile (P_{flaA} -GFP-positive) and virulent (P_{ralF} - and P_{sidC} -GFP-positive) *L. pneumophila* emerge in the cluster of non-growing bacteria within an LCV. Comparative proteomics of P_{flaA} -GFP-positive and P_{flaA} -GFP-negative *L. pneumophila* subpopulations reveals distinct proteomes with flagellar proteins or cell division proteins being preferentially produced by the former or the latter, respectively. Toward the end of an infection cycle (~ 48 h), the P_{flaA} -GFP-positive *L. pneumophila* subpopulation emerges at the cluster periphery, predominantly escapes the LCV, and spreads from the bursting host cell. These processes are mediated by the *Legionella* quorum sensing (Lqs) system. Thus, quorum sensing regulates the emergence of a subpopulation of transmissible *L. pneumophila* at the LCV periphery, and phenotypic heterogeneity underlies the intravacuolar bi-phasic life cycle of *L. pneumophila*.

Keywords flagellum; pathogen vacuole; phenotypic heterogeneity; proteome; quorum sensing

Subject Categories Membranes & Trafficking; Microbiology, Virology & Host Pathogen Interaction; Signal Transduction

DOI 10.15252/embr.202152972 | Received 30 March 2021 | Revised 1 July 2021 | Accepted 8 July 2021 | Published online 27 July 2021

EMBO Reports (2021) 22: e52972

Introduction

Clonal bacterial populations show remarkable cell-to-cell variations in the expression of phenotypic traits, a reversible phenomenon termed phenotypic heterogeneity (Ackermann, 2015; Schröter & Dersch, 2019). Examples of phenotypic variation are the “bet-hedging” and “division of labor” survival strategies, which allow the distribution of risk and gain of function at the population level by constantly developing bacterial isogenic subpopulations with different features (Diard *et al.*, 2013; Arnoldini *et al.*, 2014; Carcamo-Oyarce *et al.*, 2015; Grimbergen *et al.*, 2015; Laventie *et al.*, 2019). A prominent and clinically relevant example of phenotypic heterogeneity is the emergence of non-growing antibiotic persisters in a genetically identical bacterial population (Balaban *et al.*, 2004; Héline *et al.*, 2014; Brauner *et al.*, 2016; Conlon *et al.*, 2016; Harms *et al.*, 2016; Kortebi *et al.*, 2017; Personnic *et al.*, 2019b; Moldoveanu *et al.*, 2021). Extensive cell-to-cell variability has been also observed in infected tissues, where genetically identical pathogens deal with structured micro-environments and components of the immune system in a phenotypically heterogeneous manner (Burton *et al.*, 2014; Claudi *et al.*, 2014; Davis *et al.*, 2015; Manina *et al.*, 2015). Remarkably, heterogeneous pathogen behavior has been reported in single infected host cells indicating that phenotypic diversification occurs even among few individuals, within the micrometer range (Héline *et al.*, 2010; Campbell-Valois *et al.*, 2014; Personnic *et al.*, 2019b).

Legionella pneumophila is an amoeba-resistant environmental bacterium, which causes a severe pneumonia termed Legionnaires' disease (Newton *et al.*, 2010; Hilbi *et al.*, 2011; Mondino *et al.*, 2020). The facultative intracellular pathogen employs a conserved mechanism to grow in free-living protozoa as well as in lung macrophages (Hoffmann *et al.*, 2014; Boamah *et al.*, 2017; Swart *et al.*, 2018). Within host cells, *L. pneumophila* replicates in a unique, endoplasmic reticulum (ER)-associated compartment, the *Legionella*-containing

¹ Institute of Medical Microbiology, University of Zürich, Zürich, Switzerland

² Proteomics Core Facility, Biozentrum, University of Basel, Basel, Switzerland

³ Center for Microscopy and Image Analysis, University of Zürich, Zürich, Switzerland

⁴ Division of Inflammation and Infection, Department of Biomedical and Clinical Sciences, Linköping University, Linköping, Sweden

⁵ Division of Enteropathogenic Bacteria and Legionella, Robert Koch Institute, Wernigerode, Germany

*Corresponding author. Tel: +41 446342650; E-mail: hilbi@imm.uzh.ch

**Corresponding author. Tel: +41 446345898; E-mail: npersonnic@imm.uzh.ch

[†]These authors contributed equally to this work

[‡]Present address: Department of Quantitative Biomedicine, University of Zürich, Zürich, Switzerland

vacuole (LCV) (Asrat *et al*, 2014; Personnic *et al*, 2016; Sherwood & Roy, 2016; Steiner *et al*, 2018). LCV formation is an intricate and robust process that requires the bacterial Intracellular multiplication/Defective organelle trafficking (Icm/Dot) type IV secretion system (T4SS) and involves more than 300 different “effector” proteins, which subvert crucial host cell components and pathways (Finsel & Hilbi, 2015; Qiu & Luo, 2017).

Upon extracellular growth as well as within host cells, *L. pneumophila* adopts a bi-phasic life cycle comprising a replicative, non-virulent and a non-replicating, virulent/transmissive form (Molofsky & Swanson, 2004). The reversible switch between the two forms is tightly linked to the bacterial metabolism and nutrient availability. As nutrients become limiting, the bacteria enter the transmissive phase in a process controlled by the RNA-binding “master regulator” CsrA (Molofsky & Swanson, 2003; Sahr *et al*, 2017), the “stringent response” second messenger guanosine 3,5-bispyrophosphate (ppGpp) (Hammer & Swanson, 1999; Dalebroux *et al*, 2010), and the *Legionella* quorum sensing (Lqs) system (Tiaden *et al*, 2010a; Personnic *et al*, 2018).

In stationary growth phase, *L. pneumophila* undergoes morphological changes (Faulkner & Garduno, 2002) and produces a single monopolar flagellum (Appelt & Heuner, 2017). Accordingly, genes encoding proteins implicated in flagellum biosynthesis or the alternative sigma factor FliA (σ^{28}) are strongly upregulated under conditions of nutrient shortage (Brüggemann *et al*, 2006; Jules & Buchrieser, 2007). Transcriptomics revealed that the alternative (stress response) sigma factor RpoS (σ^{38}) positively controls the regulation of *fliA* as well as *flaA*, encoding the major flagellum component, flagellin (Hovel-Miner *et al*, 2009). Moreover, the *L. pneumophila* small signaling molecule *Legionella* autoinducer-1 (LAI-1) and the Lqs system regulate *P_{flaA}* expression and FlaA production as well as bacterial motility (Schell *et al*, 2016b; Hochstrasser & Hilbi, 2017).

The Lqs system comprises the autoinducer synthase LqsA, which produces the α -hydroxyketone compound LAI-1 (3-hydroxypentadecane-4-one) (Spirig *et al*, 2008), the cognate membrane-bound sensor histidine kinases LqsS (Tiaden *et al*, 2010b) and LqsT (Kessler *et al*, 2013), and the prototypic response regulator LqsR (Tiaden *et al*, 2007; Tiaden *et al*, 2008), which dimerizes upon LqsS- and LqsT-mediated phosphorylation (Schell *et al*, 2014; Schell *et al*, 2016b; Hochstrasser *et al*, 2020). The Lqs system regulates a number of *L. pneumophila* traits (Personnic *et al*, 2018), including virulence (Tiaden *et al*, 2007; Tiaden *et al*, 2008), pathogen and host cell motility (Simon *et al*, 2015; Schell *et al*, 2016b), and natural competence for DNA uptake (Kessler *et al*, 2013), as well as the switch from the replicative to the virulent/transmissive phase (Tiaden *et al*, 2007). Recent studies revealed that the Lqs system also regulates the phenotypic heterogeneity of *L. pneumophila* in amoeba and macrophages (Personnic *et al*, 2019b), as well as in biofilms and microcolonies (Personnic *et al*, 2021). Accordingly, quorum sensing modulates the formation of subpopulations of metabolically active virulent persisters within infected cells and regulates the persistence, resuscitation, and virulence of sessile *L. pneumophila* in biofilms.

In this study, we analyzed on a single-cell level the timing and emergence of individual transmissive *L. pneumophila* bacteria in the LCV at late stages of infection. Intravacuolar *L. pneumophila* clusters developed a spatially organized motile subpopulation primarily at the cluster periphery. The Lqs system controlled the

emergence of the motile subpopulation, which preferentially escaped the LCV and spread from the destroyed host cell, while non-motile bacteria were left behind. Hence, Lqs-regulated phenotypic heterogeneity underlies bet-hedging as well as division of labor strategies employed by *L. pneumophila* subpopulations toward the end of an infection cycle in the host cell.

Results

Intravacuolar *L. pneumophila* clusters develop spatially organized subpopulations

Upon internalization by phagocytic cells, *L. pneumophila* forms a customized vacuolar niche, the LCV, wherein the bacterium either resumes clonal growth or enters non-replicating persistence (Personnic *et al*, 2019b). The kinetics, cues, and functional consequences of phenotypic heterogeneity of intracellular *L. pneumophila* are not well understood. In order to delineate intracellular phenotypic heterogeneity, we used the dual fluorescence reporter construct *P_{tac}-mCherry-P_{flaA}-gfp*, which produces mCherry constitutively and GFP under the control of the *P_{flaA}* promoter. The *P_{flaA}*-dependent production of GFP serves as a proxy for motility and the switch to the transmissive phase of *L. pneumophila* (Personnic *et al*, 2019b). In broth, the majority of wild-type *L. pneumophila* JR32 (*P_{tac}-mCherry-P_{flaA}-gfp*) showed a low fluorescence ratio around 500 nm/600 nm (red fluorescent) in the exponential growth phase (17 h) and a high fluorescence ratio (green fluorescent) in the stationary phase (26 h; Appendix Fig S1A), in agreement with switching from the replicative to the transmissive phase.

To study the bi-phasic life cycle transition during an infection in detail, we sought to assess the emergence and spatial distribution of transmissive *L. pneumophila* on a single-cell level. To this end, we infected *Acanthamoeba castellanii* amoebae with wild-type strain JR32 harboring the *P_{tac}-mCherry-P_{flaA}-gfp* reporter construct and monitored the GFP production by fluorescence microscopy (Fig 1A, Appendix Fig S2A). The stationary phase bacterial liquid culture used as an inoculum for the infections homogeneously produced GFP (Personnic *et al*, 2021). At 6 h post-infection (p.i.), some of the bacteria still remained in the transmissive phase (high levels of GFP production; green fluorescent), while others had resumed growth (low/no GFP production; red fluorescent). At later time points, all the intracellular bacteria were replicating and formed clusters, which did not produce any GFP (24, 30 h p.i.). At 42 h p.i., a few single bacteria located in the periphery of the intracellular microcolony started to produce GFP, indicating that they had switched to the transmissive phase. Within a short period of time, the bacterial cluster became covered by GFP-producing, transmissive *L. pneumophila*, but the phenotypic conversion was predominantly occurring in peripheral bacteria (48 h p.i.; Fig 1A, Appendix Fig S2A). Flow cytometry-based analysis confirmed that upon growth in *A. castellanii*, the majority of wild-type *L. pneumophila* was red fluorescent at an earlier time point (24 h p.i.) and green fluorescent at a later time point (48 h p.i.; Appendix Fig S1B).

Many *L. pneumophila* Icm/Dot-translocated effector proteins, including the well-studied effector proteins RalF or SidC, are produced in stationary growth phase (Nagai *et al*, 2002; Luo & Isberg, 2004). As a proxy for *L. pneumophila* virulence, we

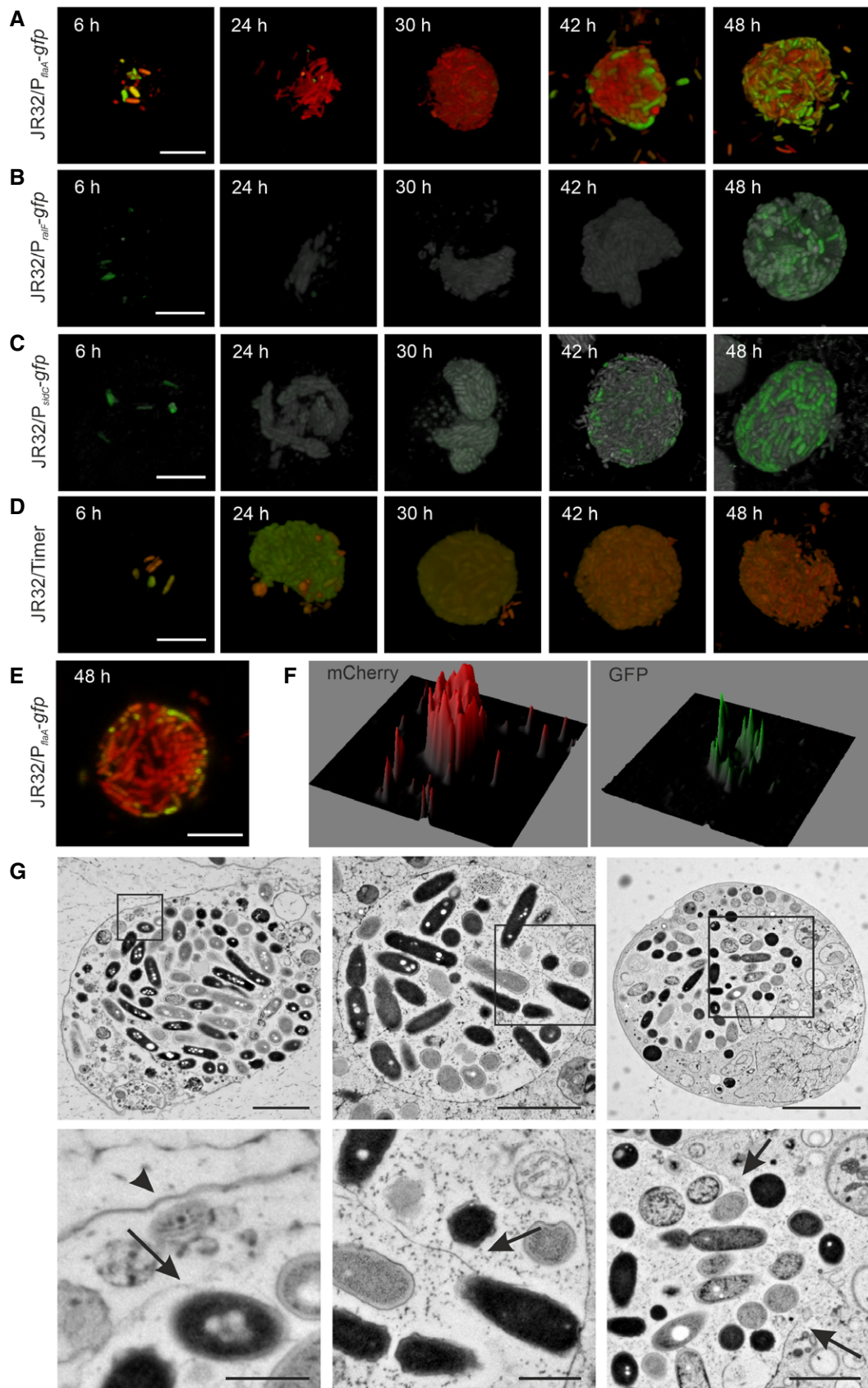


Figure 1.

Figure 1. Intravacuolar *Legionella pneumophila* clusters develop spatially organized subpopulations.

- A–D *Acanthamoeba castellanii* was infected (MOI 5) with *L. pneumophila* JR32 producing (A) GFP under the control of P_{flaA} (P_{tac} -mCherry- P_{flaA} -*gfp*) and mCherry constitutively, (B) GFP under the control of P_{ralF} (P_{ralF} -*gfp*) and stained with DAPI, (C) GFP under the control of P_{sidC} (P_{sidC} -*gfp*) and stained with DAPI, or (D) Timer constitutively (pNP107). The infected amoebae were fixed at different time points post-infection and analyzed by confocal microscopy and 3D reconstructed (scale bars: 5 μ m). Motile and virulent bacteria (GFP-positive) emerged at the colony cluster periphery only after bacterial replication had ceased (red fluorescent Timer).
- E, F Optical section (E) (scale bar: 5 μ m) and distribution of the fluorescence signal intensity (F) of *A. castellanii* infected with mCherry-producing *L. pneumophila* JR32 (P_{tac} -mCherry- P_{flaA} -*gfp*) for 48 h. The plot profile was analyzed for an optical section in the center of an infected host cell and shows the intensity of the green and red channels, respectively (representative of $n = 10$). The GFP signal mainly localizes to the periphery of the bacterial cluster.
- G Transmission electron micrographs of *A. castellanii* infected with *L. pneumophila*. *Acanthamoeba castellanii* was infected (MOI 5, 42 h) with *L. pneumophila* wild-type strain JR32 and subjected to high-pressure freezing and electron microscopy. Many LCVs were still intact at 42 h post-infection (left panel; arrow: intact LCV membrane, arrowhead plasma membrane), and occasionally, the bacteria were flagellated (middle panel, arrow). Some LCVs were already ruptured, and the bacteria were released into the host cell cytosol (right panel; arrows: ruptured LCV membrane). Scale bars: 2 μ m and 0.5 μ m (insets).

employed transcriptional fusions of *gfp* with the P_{ralF} or P_{sidC} promoters, which control the production of RalF and SidC, respectively. Beyond 6 h p.i., wild-type *L. pneumophila* harboring a P_{ralF} -*gfp* (Fig 1B, Appendix Fig S2B) or P_{sidC} -*gfp* (Fig 1C, Appendix Fig S2C) reporter construct replicated and formed intravacuolar clusters. However, GFP was not produced until very late during infection (42–48 h p.i.), where GFP-positive bacteria appeared throughout the cluster. Of note, at early time points (6 h p.i.) most amoebae contained only one or a few bacteria, which were positive for P_{ralF} -*gfp* or P_{sidC} -*gfp*, respectively. This observation is in agreement with the notion that these bacteria are virulent (amoeba-resistant) and still in stationary growth phase.

To correlate P_{flaA} , P_{ralF} , or P_{sidC} induction with bacterial growth, we monitored the production of the fluorescent protein Timer during infection (Personnic *et al.*, 2019b). Upon production by growing bacteria, the Timer protein quickly adopts a green fluorescent conformation and slowly matures into a red fluorescent variant in non-growing bacteria. Intracellular growth of *L. pneumophila* was observable up to 30 h p.i., as indicated by the prevalence of green fluorescent Timer. However, at 42–48 h p.i. only non-growing bacteria harboring red fluorescent Timer were found in the clusters (Fig 1D, Appendix Fig S2D). Hence, the production and spatial heterogeneity of P_{flaA} , P_{ralF} , or P_{sidC} induction was observed well after the bacteria had ceased to grow. In summary, P_{flaA} , P_{ralF} , and P_{sidC} show a bistable expression pattern at late stages of *L. pneumophila* infection, indicating that individual bacteria, which express these markers, are motile and virulent.

To have a more detailed look at the distribution of the fluorescence signal within the intracellular bacterial clusters, a single optical section in the middle of the infected cell was selected (Fig 1E), and 3D histograms were generated based on the signal intensity from the individual green and red fluorescent channels (Fig 1F). This approach confirmed that the GFP-positive, transmissible bacteria were located at the periphery of the bacterial cluster, while mCherry-producing bacteria were distributed throughout the cluster. Using live-cell fluorescence microscopy of *L. pneumophila*-infected *A. castellanii*, we did not observe intravacuolar bacterial motility in the clusters, and therefore, the peripheral location of the GFP-producing bacteria was not due to bacterial movement within the LCV (Movies EV1–EV6). Given the rather static features and the three-dimensional organization of the intravacuolar bacterial assemblages, the clusters might be regarded as “microcolonies”.

Since the fluorescent protein mCherry is quite stable, it might outlive a protein production shutdown for some time, and the interior bacteria might not produce GFP because of an overall lack of protein

production. To address this question, we conducted fluorescence recovery after photobleaching (FRAP) experiments (Appendix Fig S1C). This approach indicated that the interior bacteria indeed synthesized mCherry *de novo*, ruling out the possibility that these bacteria did not produce GFP because overall protein production ceased. In contrast, treatment of the infected cells with the ribosome inhibitor erythromycin did shut down protein synthesis.

Electron microscopy (EM) analysis revealed that at 42 h p.i., 62% of the LCVs ($n = 21$) harboring densely packed wild-type *L. pneumophila* were intact (Fig 1G, left panel), and occasionally, the bacteria were flagellated (Fig 1G, middle panel). At this time point, 38% of the pathogen vacuoles were already ruptured, and the bacteria were released into the host cell cytosol (Fig 1G, right panel). These ultrastructural studies also indicated some morphological heterogeneity and differential staining of the intravacuolar bacteria. The expression of P_{flaA} -*gfp* was confirmed by anti-GFP immunogold EM (Appendix Fig S1D). Using this approach, 27% wild-type *L. pneumophila* expressing *gfp* under the control of the P_{flaA} promoter (JR32/ P_{tac} -mCherry- P_{flaA} -*gfp*) produced GFP (average 0.33 GFP/bacterium, $n = 255$), while 92% wild-type bacteria constitutively expressing *gfp* (JR32/pNT28) produced GFP (average 3.12 GFP/bacterium, $n = 217$). Taken together, while flagella and P_{flaA} -controlled GFP were only rather rarely identified, the results suggest that at late stages of infection some intravacuolar *L. pneumophila* are motile.

Finally, to determine whether bistable P_{flaA} expression is restricted to amoebae or whether phenotypic heterogeneity is also observable in mammalian cells, we infected RAW 264.7 macrophages at 37°C for 18–28 h with *L. pneumophila* harboring the reporter construct P_{tac} -mCherry- P_{flaA} -*gfp* (Fig EV1). Under these conditions, a subpopulation of bacteria expressed P_{flaA} -*gfp* only at late stages of infection (28 h) in macrophages, similar to what was observed in amoebae. Therefore, the infection of evolutionarily distant macrophages and amoebae with *L. pneumophila* at different temperatures yielded essentially the same pattern of bistable P_{flaA} expression in the bacteria.

To establish the reversible nature of the intracellular phenotypic cell-to-cell variations, we sorted by flow cytometry subpopulations of *L. pneumophila* JR32/ P_{tac} -mCherry- P_{flaA} -*gfp* from lysates of *A. castellanii* infected for 42 h according to the GFP production level (i.e., P_{flaA} -GFP-positive and P_{flaA} -GFP-negative; Appendix Fig S3A), and the sorted subpopulations were used to infect *A. castellanii* for 42 h. Upon re-infection of *A. castellanii*, each of the sorted subpopulations again produced P_{flaA} -GFP-positive and P_{flaA} -GFP-negative subpopulations with the same spatial distribution and size

as pre-sort bacteria (Appendix Fig S3B). Moreover, imaging flow cytometry (IFC) analysis confirmed that the green fluorescence intensity varied greatly at late time points of infection, while the intensity of the red fluorescence (constitutively produced mCherry) was similar for all bacteria imaged (Appendix Fig S3C). In summary, at late stages of infection, *L. pneumophila* develops intravacuolar clusters in amoebae and macrophages showing heterogeneity (bistability) in P_{flaA} -*gfp* expression. The transcriptional differentiation is reversible and spatially organized, as P_{flaA} -GFP-positive (transmissive) individuals emerge at the periphery of the bacterial clusters.

The intravacuolar *L. pneumophila* subpopulations produce distinct proteomes

In order to further characterize the intravacuolar *L. pneumophila* subpopulations on a biochemical level, we analyzed P_{flaA} -GFP-positive and P_{flaA} -GFP-negative bacteria by comparative proteomics. To this end, *A. castellanii* infected with *L. pneumophila* JR32/ P_{tac} -*mCherry-P_{flaA}-gfp* were lysed with detergent after 42 h of infection, sorted by fluorescence-activated cell sorting (FACS), and subjected to proteomics analysis (Fig 2A). After sorting, the P_{flaA} -GFP-positive and P_{flaA} -GFP-negative subpopulations were 80–90% pure (Appendix Fig S3A).

Using this approach, we identified more than 800 proteins produced in the P_{flaA} -GFP-positive and P_{flaA} -GFP-negative *L. pneumophila* populations (Fig 2A, Dataset EV1). The P_{flaA} -GFP-positive *L. pneumophila* population preferentially produced proteins implicated in the production and assembly of the flagellum (FlaA, FlgD, FlgE, FliA, FliS, FleQ; Fig 2B). These findings validate that P_{flaA} -GFP-positive bacteria indeed produce flagellin (FlaA) and correspond to the occasional observation of intracellular flagellated bacteria by EM (Fig 1G, middle panel). Furthermore, the results are in agreement with the notion that the P_{flaA} -GFP-positive intravacuolar *L. pneumophila* subpopulation is motile. The P_{flaA} -GFP-positive subpopulation also produced the replication inhibitors MinD and MinC. In contrast, the P_{flaA} -GFP-negative subpopulation produced the proteins FtsZ, FtsA, and MinE, which promote cell division and replication (Fig 2C). Hence, bacterial replication appears to have ceased in the P_{flaA} -GFP-positive population, while it might still take place at a low rate in the P_{flaA} -GFP-negative population, despite the Timer fluorescence ratio corresponding to non-growing bacteria (Fig 1D).

In order to further validate the proteomics data, we sought to analyze the expression of genes corresponding to differentially produced proteins. A protein massively produced by the P_{flaA} -GFP-positive *L. pneumophila* subpopulation is the major regulator of the flagellar regulon, FleQ (Albert-Weissenberger *et al*, 2010; Schulz *et al*, 2012). In contrast, a protein mainly produced by the P_{flaA} -GFP-negative population is LegC8 (Lpg2862, Lgt2). LegC8 is a eukaryote-like protein and an Icm/Dot substrate (de Felipe *et al*, 2005; de Felipe *et al*, 2008), which is toxic/growth inhibitory for yeast (de Felipe *et al*, 2008) by acting as a translation inhibitor targeting the elongation factor eEF1A (Hurtado-Guerrero *et al*, 2010; Belyi *et al*, 2013; Inaba *et al*, 2019). Interestingly, LegC8 is produced in the post-exponential growth phase by *L. pneumophila* growing in broth (Aurass *et al*, 2016). To test the intravacuolar expression of the *fleQ* or *legC8* genes, we generated the reporter constructs P_{fleQ} -*mCherry-P_{flaA}-gfp* and P_{legC8} -*mCherry-P_{flaA}-gfp*, and we infected *A. castellanii* with *L. pneumophila* wild-type strains producing

these reporters. The expression studies confirmed that at late stages of infection (48 h p.i.), P_{fleQ} -mCherry is produced along with P_{flaA} -GFP in most bacteria (Fig 2D), while bacteria harboring the P_{legC8} -*mCherry-P_{flaA}-gfp* construct preferentially produce either P_{legC8} -mCherry or P_{flaA} -GFP, but not both (Fig 2E).

Finally, we tested whether the P_{flaA} -GFP-positive and P_{flaA} -GFP-negative subpopulations differ with regard to viability (Appendix Fig S3D), intracellular replication in *A. castellanii* (Appendix Fig S3E), or antibiotics tolerance (Appendix Fig S3F). Under the conditions used, the P_{flaA} -GFP-positive and P_{flaA} -GFP-negative subpopulations did not show any significant differences. Given that these bacteria are essentially non-replicating (Fig 1D), they likely are persisters. In summary, the P_{flaA} -GFP-positive and P_{flaA} -GFP-negative intracellular *L. pneumophila* subpopulations are characterized by distinct proteomes, specifically comprising structural or regulatory flagellar proteins, or cell division proteins and distinct effectors, respectively.

Preferential exit of motile *L. pneumophila* from LCVs and host cells

Acanthamoeba castellanii is an environmental and natural host of *L. pneumophila*, wherein robust bacterial growth is observed. Accordingly, an infection/growth temperature of 25°C likely occurs in the environment and is physiologically relevant. The conditions of 25°C/48 h p.i. reflect the status when an infection cycle is nearly completed and heterogeneity in P_{flaA} expression is clearly visible. Infection of *A. castellanii* with *L. pneumophila* for approximately 48 h revealed that some bacteria remained confined to the LCV (Fig 1G, first panel), even after phenotypic conversion of a P_{flaA} expressing subpopulation at the cluster periphery had occurred (Fig 1A). Using P_{flaA} expression (GFP production) as a proxy for motility, we next sought to functionally validate the expression pattern and correlate the phenotypic heterogeneity with virulence traits. To investigate the functional relevance of peripheral P_{flaA} -GFP-positive *L. pneumophila* at late stages of infection of *A. castellanii*, we tested whether the emergence of these motile bacteria correlates with LCV membrane rupture, as observed by EM (Fig 1G, last panel), and/or with host cell lysis. To this end, we assessed the infection and lysis processes by live-cell microscopy (Appendix Fig S4A, Movie EV1). Strikingly, upon LCV membrane rupture, motile bacteria escaped to the host cell cytosol and caused an “explosive” lysis of the host cell within minutes if not seconds. These observations suggested that *L. pneumophila* concludes the cellular infection cycle with a rapid two-step process, comprising (i) LCV escape and (ii) host cell lysis.

To further analyze this process, we took advantage of the genetically tractable amoeba *Dictyostelium discoideum*, allowing the ectopic production of fluorescently labeled proteins of interest. *Dictyostelium discoideum* was infected for ca. 48 h with wild-type *L. pneumophila* harboring the P_{tac} -*mCherry-P_{flaA}-gfp* reporter construct, and the infection was monitored by real-time microscopy (Fig 3A, Appendix Fig S5A, Movie EV2). Similar to *A. castellanii*, the LCV exit of *L. pneumophila* in *D. discoideum* coincided with the emergence of P_{flaA} -GFP-positive bacteria at the rupture site, and the first bacterium escaping the pathogen vacuole generally belonged to the P_{flaA} -GFP-positive subpopulation (Fig 3A, Appendix Fig S5A, Movie EV2, 0 s). In fact, in all the instances ($n = 4$), where the onset of LCV escape was captured by real-time microscopy, a

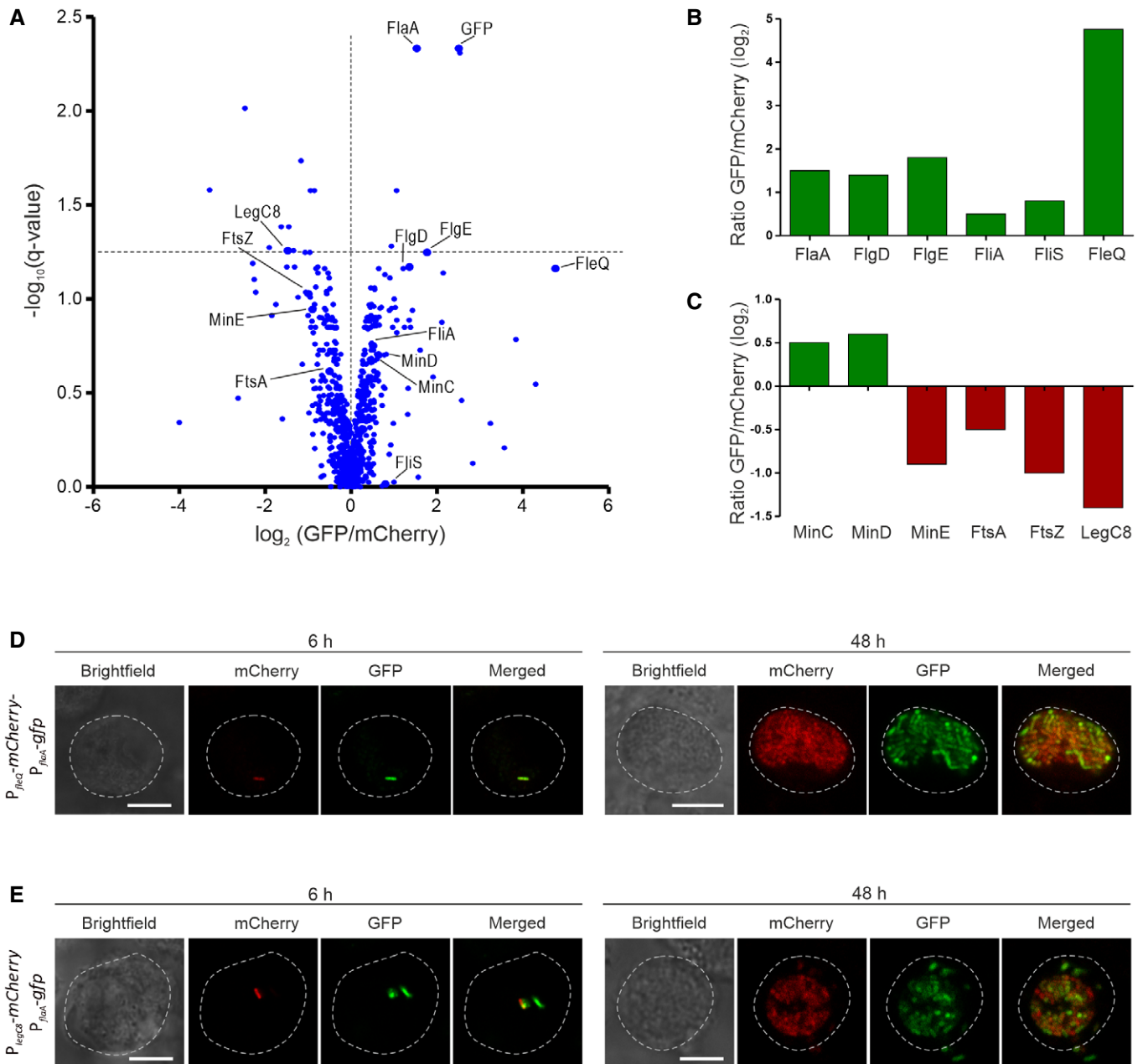


Figure 2. The intravacuolar *Legionella pneumophila* subpopulations produce distinct proteomes.

- A** *Legionella pneumophila* subpopulation proteomics. *Acanthamoeba castellanii* was infected (MOI 5, 42 h) with *L. pneumophila* JR32 ($P_{tac}\text{-mCherry-}P_{flaA}\text{-gfp}$). After cell lysis, released intracellular bacteria were sorted by flow cytometry in mCherry-positive/GFP-negative and mCherry-positive/GFP-positive *L. pneumophila* subpopulations, and their proteome was determined and compared. Protein abundance in each subset is depicted as a volcano plot. Proteins enriched in the GFP-producing subpopulation have a positive \log_2 ratio (and a low q -value).
- B, C** The ratio (GFP/mCherry) of selected proteins is indicated for (B) proteins relevant for flagellum formation and (C) cell division proteins and a T4SS substrate (LegC8). The ratio of the mean intensities from three independent proteomics experiments is shown.
- D, E** Expression of select *L. pneumophila* genes in amoebae. *Acanthamoeba castellanii* was infected (MOI 5; 6 and 48 h) with *L. pneumophila* JR32 harboring reporter constructs for (D) $P_{flaQ}\text{-mCherry-}P_{flaA}\text{-gfp}$ or (E) $P_{legC8}\text{-mCherry-}P_{flaA}\text{-gfp}$, respectively. The infected amoebae were fixed and imaged by confocal microscopy (scale bars: 5 μm).

P_{flaA} -GFP-positive bacterium was the first to exit the pathogen vacuole. Analogously, host cell lysis and subsequent exit of *L. pneumophila* to the extracellular milieu coincided with the accumulation

of motile bacteria at the plasma membrane, and the first bacterium escaping the host cell was P_{flaA} -GFP-positive (Fig 3A, Appendix Fig S5A, Movie EV2, 185 s). In all instances observed by real-time

microscopy ($n = 8$), a P_{flaA} -GFP-positive bacterium was the first to leave the lysed host cell.

The exit of *L. pneumophila* to the extracellular milieu was associated with host cell perforation and likely cell death, as indicated by leakage of the cytosolic red fluorescent protein mCherry from the amoebae (Fig 3B, Movie EV3). Noteworthy, the loss of cytosolic mCherry coincided in more than 90% of the cases ($n = 22$) with the escape of *L. pneumophila* from the host cell ($n = 20$). In $< 10\%$ of the cases, the loss of cytosolic mCherry preceded *L. pneumophila* evasion from the LCV and host cell (Appendix Fig S5B, Movie EV4). In these cases, the first bacterium to exit the pathogen vacuole was not necessarily P_{flaA} -GFP-positive ($n = 2$). These results imply that the release of the pathogen triggers host cell perforation and death, rather than host cell perforation and death allows the release of the pathogen.

In order to enhance the visibility of LCV integrity during the escape process, we employed *D. discoideum* producing the LCV/PtdIns(4)*P* probe P4C-mCherry, which distinctively labels the LCV membrane, or an amoeba strain producing cytosolic mCherry, which is excluded from the lumen of intact LCVs. Infecting these *D. discoideum* strains with *L. pneumophila* constitutively producing mCerulean and P_{flaA} -GFP for ca. 48 h revealed that the LCV integrity was not compromised prior to bacterial exit, as indicated by a continuous P4C-mCherry-positive LCV membrane or the exclusion of cytosolic mCherry (Appendix Fig S5C and D). The exit of P_{flaA} -GFP-positive *L. pneumophila* from LCVs caused the local rupture of the P4C-mCherry-positive pathogen vacuole membrane (Fig 3C, Movie EV5) and influx of cytosolic mCherry into the LCV lumen, as well as loss of cytosolic mCherry indicating host cell lysis (Fig 3D, Movie EV6). In summary, independently of the *D. discoideum* and bacterial reporter strains used, the P_{flaA} -GFP-positive bacteria preferentially escaped the LCV and/or the host cell. Accordingly, P_{flaA} -GFP-positive *L. pneumophila* appear to actively rupture the LCV and the plasma membrane.

P_{flaA} -GFP-positive individual *L. pneumophila* bacteria preferentially contacted the LCV and plasma membrane rupture sites, and therefore, FlaA might be implicated in active membrane lysis. To test this hypothesis, we infected *D. discoideum* (Fig 3E) or *A. castellanii* (Appendix Fig S4B) with an *L. pneumophila* mutant strain lacking the major flagellum component flagellin, FlaA ($\Delta flaA$) (Weber et al, 2012). Live-cell microscopy analysis performed at ca. 48 h p.i. revealed that the $\Delta flaA$ mutant strain ruptured both the LCV and the plasma membrane of either *D. discoideum* or *A. castellanii*. However, the process appeared less vigorous, and the mutant bacteria remained clustered at the exit site, and due to the lack of a functional flagellum did not spread into the environment (Fig 3E, Appendix Fig S4B, Movies EV7 and EV8). Taken together, the presence of transmissible *L. pneumophila* at the LCV and plasma membranes correlates with pathogen vacuole rupture and preferential exit of this bacterial subpopulation from the lysed host cell. A functional flagellum appears not essential for the process.

Selective spread of the motile *L. pneumophila* subpopulation from lysed *A. castellanii*

To further assess the functional consequences of heterogeneous P_{flaA} -GFP expression, we tested the spreading of the motile *L. pneumophila* subpopulation from infected amoebae immobilized in

agarose (Personnic et al, 2019a). To this end, *A. castellanii* were infected with *L. pneumophila* harboring the P_{tac} -mCherry- P_{flaA} -gfp reporter construct and embedded in 0.5% agarose/PYG. From ca. 30 h p.i., the infected amoebae were monitored an additional 72 h by real-time microscopy. Around 46 h p.i., peripheral P_{flaA} -GFP-positive (motile) *L. pneumophila* emerged in an intracellular bacterial cluster. Within 1.5 h, ca. 60% of the bacteria had converted to P_{flaA} -GFP-positive individuals, which covered the cluster and subsequently spread from the bursting amoeba (Fig 4A, Movie EV9). Toward the end of the infection (> 55 h p.i.), primarily mCherry-positive/GFP-negative (non-motile) *L. pneumophila* remained clustered among the cellular debris.

Next, we quantified the number and the spreading distance of *L. pneumophila* wild-type or mutant strains released from lysed amoebae (Fig 4B). The $\Delta flaA$ mutant strain (Weber et al, 2012) lacks flagellin (FlaA) and accordingly is non-motile. *Acanthamoeba castellanii* amoebae were infected with *L. pneumophila* JR32 or $\Delta flaA$ harboring the P_{tac} -mCherry- P_{flaA} -gfp reporter construct and embedded in 0.5% agarose/PYG for 52 h, at which time point most if not all of the infected amoebae had already burst and released the intracellular bacteria (JR32: 96%, $\Delta flaA$: 100%) Real-time imaging revealed that *L. pneumophila* $\Delta flaA$ did not spread at all, and the GFP-positive mutant bacteria remained attached to the mCherry-producing bacterial cluster (Fig 4B). Quantification of the number of released bacteria indicated that compared to the parental strain approximately 25-fold less $\Delta flaA$ mutant bacteria spread from the lysed host cells (Fig 4C, Appendix Fig S6D), and the spreading distance of the mutant bacteria was at least eight-fold shorter (Fig 4D, Appendix Fig S6E).

Analogous experiments were performed with the $\Delta lqsA$ mutant strain (Spirig et al, 2008), which lacks the autoinducer synthase LqsA and does not produce the quorum sensing signaling molecule LAI-1. The pleiotropic Lqs system regulates *L. pneumophila* virulence and transmissible traits, including the expression of *flaA* and bacterial motility (Schell et al, 2016b). While most of the $\Delta lqsA$ -infected amoebae bursted (ca. 90%), the release of $\Delta lqsA$ mutant bacteria from agarose-embedded *A. castellanii* was severely impaired (Fig 4B), and compared to the parental strain JR32 about three times less mutant bacteria were released from the destroyed amoebae (Fig 4C) with a significantly shorter spreading distance (Fig 4D). These findings are in agreement with the notion that LqsA regulates the spread of the motile *L. pneumophila* subpopulation at late states during infection. In summary, the peripheral P_{flaA} -GFP-positive *L. pneumophila* subpopulation represents the motile fraction of intravacuolar *L. pneumophila*, which preferentially and independently of the flagellum (FlaA) escapes amoebae and dependent on the flagellum spreads to the environment.

The Lqs system regulates the emergence and LCV escape of the motile *L. pneumophila* subpopulation

The Lqs system regulates the formation of intracellular *L. pneumophila* persists (Personnic et al, 2019b) and is implicated in the spread of the motile *L. pneumophila* subpopulation from host cells (Fig 4). Based on these findings, we sought to characterize in detail the role of the Lqs system for spatial expression of P_{flaA} in LCVs and the function of the corresponding subpopulation at late stages of infection. To this end, *A. castellanii* were infected for 48 h with

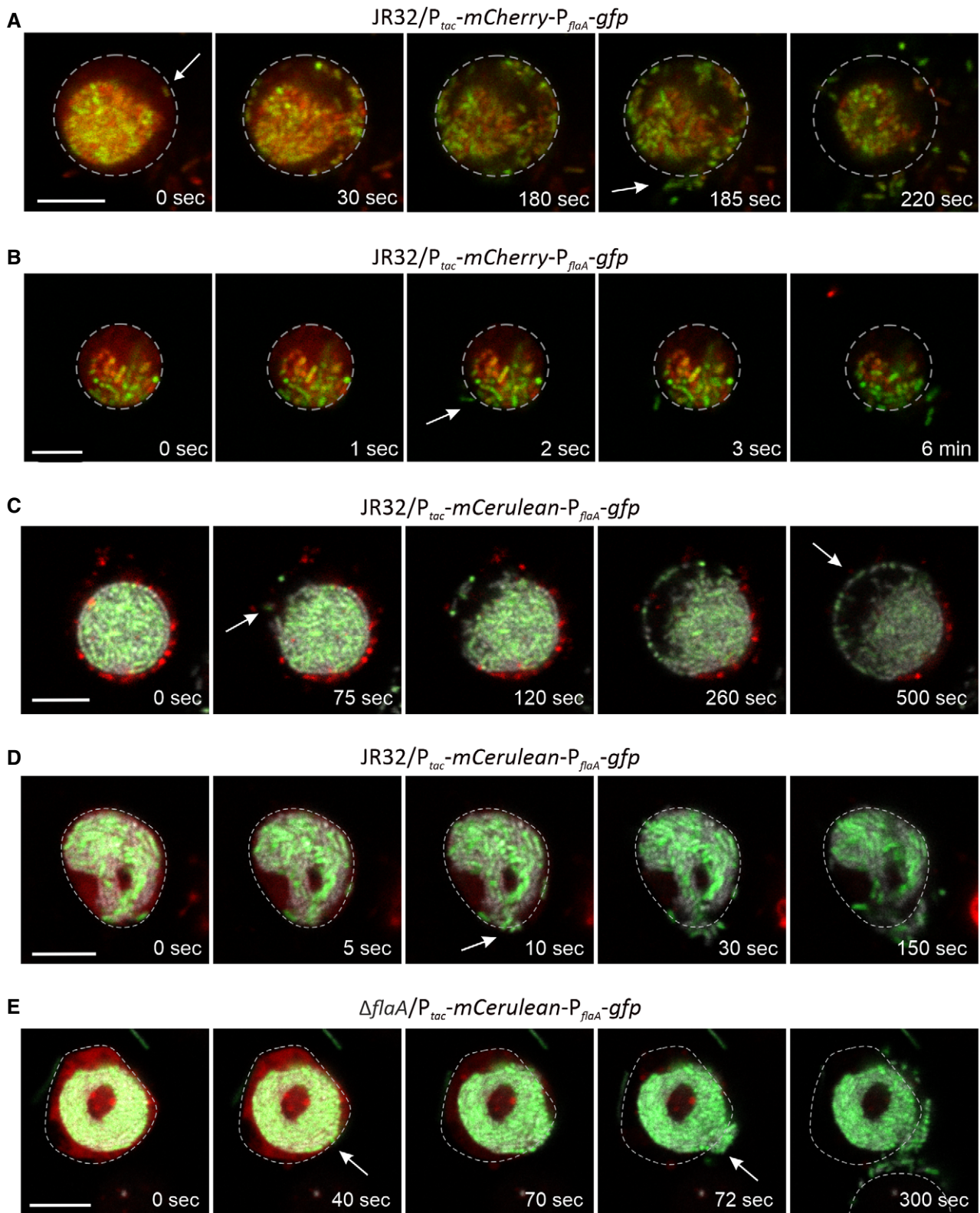


Figure 3.

Figure 3. Preferential exit of the motile *Legionella pneumophila* subpopulation.

A–E Representative live-cell microscopy images of *Dictyostelium discoideum* infected with P_{flaA} -GFP-producing *L. pneumophila*. *Dictyostelium discoideum* Ax3 producing cytosolic mCherry (pDM1042) was infected (MOI 5) with (A, B) wild-type *L. pneumophila* JR32 (P_{tac} -mCherry- P_{flaA} -gfp), (C, D) JR32 (P_{tac} -mCerulean- P_{flaA} -gfp) or (E) $\Delta flaA$ (P_{tac} -mCerulean- P_{flaA} -gfp) and embedded in agarose for 48 h. P_{flaA} -GFP-positive *L. pneumophila* (A) escape the LCV (0 s), followed by other bacteria, which are contained in the cytosol and localize to the plasma membrane, where a P_{flaA} -GFP-positive *L. pneumophila* first leaves the ruptured host cell (185 s), or (B) triggers host cell death (loss of cytosolic mCherry) upon exit of the amoeba. P_{flaA} -GFP-positive *L. pneumophila* (C) escape the LCV (75 s) and spread within the cytosol for several minutes, and (D) are the first to exit the host cell, leading to the loss of cytosolic mCherry and host cell death. (E) *L. pneumophila* $\Delta flaA$ lyses the LCV and host cell less vigorously. Scale bars: 5 μ m.

wild-type *L. pneumophila* JR32, $\Delta lqsA$, $\Delta lqsR$, $\Delta lqsS$, $\Delta lqsT$, or $\Delta lqsS$ - $\Delta lqsT$ harboring the P_{tac} -mCherry- P_{flaA} -gfp reporter construct, fixed, and analyzed by high-resolution fluorescence microscopy. Under these conditions, the $\Delta lqsA$, $\Delta lqsR$, and $\Delta lqsS$ - $\Delta lqsT$ mutant strains produced fewer GFP-positive bacteria in the intravacuolar bacterial clusters compared to wild-type bacteria (Fig 5A, Appendix Fig S6A). For quantification, *A. castellanii* were infected for 48 h with *L. pneumophila* JR32, $\Delta lqsA$, $\Delta lqsR$, $\Delta lqsS$, $\Delta lqsT$, or $\Delta lqsS$ - $\Delta lqsT$ harboring the P_{tac} -mCherry- P_{flaA} -gfp reporter construct, lysed by detergent, fixed, and analyzed by flow cytometry. This approach confirmed that the $\Delta lqsA$, $\Delta lqsR$, and $\Delta lqsS$ - $\Delta lqsT$ mutant strains indeed produced 10–20% fewer GFP-positive bacteria compared to the parental strain, while the $\Delta lqsS$ and $\Delta lqsT$ mutants formed 5–10% more GFP-positive bacteria (Fig 5B).

In order to also analyze an earlier time point post-infection, we infected *A. castellanii* for 42 h p.i. with *L. pneumophila* JR32, $\Delta lqsA$, $\Delta lqsR$, $\Delta lqsS$, $\Delta lqsT$, or $\Delta lqsS$ - $\Delta lqsT$ harboring the P_{tac} -mCherry- P_{flaA} -gfp (Appendix Fig S6B and C). Under these conditions, the overall number of P_{flaA} -positive bacteria was ca. 30% lower for all strains compared to the 48 h time point, but the pattern among the strains was essentially the same as at 48 h p.i. Taken together, the components of the Lqs system regulate the emergence of P_{flaA} -GFP-positive *L. pneumophila* in intravacuolar bacterial clusters at late time points during infection.

To test a possible role of the Lqs system for LCV rupture and the resultant localization of *L. pneumophila* in the cytosol, we assessed ubiquitination of the bacteria, which occurs upon lysis of the pathogen vacuole (Koliwer-Brandl et al, 2019). To this end, *A. castellanii* was infected for 48 h with *L. pneumophila* JR32, $\Delta lqsA$, $\Delta lqsR$, $\Delta lqsS$, $\Delta lqsT$, or $\Delta lqsS$ - $\Delta lqsT$ mutant strains, fixed, and immuno-labeled for ubiquitin. Subsequently, the amoebae harboring ubiquitinated bacteria were quantified by fluorescence microscopy (Fig 5C). In more than 30% of the amoebae infected with *L. pneumophila* JR32, the bacteria stained positive for ubiquitin, i.e., their LCVs were lysed (Fig 5D). In contrast, only about 8–12% of *A. castellanii* infected with an *lqs* mutant strain contained ubiquitin-decorated bacteria. Accordingly, approximately 3- to 4-fold fewer *A. castellanii* amoebae harbored ubiquitinated *lqs* mutant bacteria, as compared to *L. pneumophila* wild-type.

In analogous experiments, we also tested the role of the Lqs system for LCV escape in *D. discoideum* (Fig 5E). In approximately 13% of these amoebae infected with wild-type *L. pneumophila*, the bacteria stained positive for ubiquitin, and therefore, their LCVs were lysed (Fig 5F). In contrast, less than 2–4% of the amoebae infected with an *lqs* mutant strain contained ubiquitin-decorated bacteria. Accordingly, approximately 3- to 6-fold fewer *D. discoideum* amoebae harbored ubiquitinated *lqs* mutant bacteria, as compared to *L. pneumophila* wild-type.

In order to confirm that ubiquitination indeed is a valid proxy for LCV lysis, we employed a *D. discoideum* strain producing the LCV membrane/PtdIns(4)P probe P4C-GFP and cytosolic mCherry as markers of LCV and plasma membrane integrity, respectively (Fig 5G). Using this approach, the parental strain JR32 localized in intact LCV/intact cell (18.5%), lysed LCV/lysed cell (60.2%), lysed LCV/intact cell (15.5%), or intact LCV/lysed cell (5.8%). Compared to intact amoebae infected by JR32, about twice as many intact amoebae hosting an *lqs* mutant strain harbored intact LCVs (Fig 5H). This was also the case for *D. discoideum* hosting $\Delta flaA$ mutant *L. pneumophila*, indicating that the flagellum (FlaA) indeed contributes to LCV lysis. Taken together, the Lqs system promotes LCV rupture and cytosolic localization of *L. pneumophila* in *A. castellanii* as well as in *D. discoideum*, and therefore, quorum sensing regulates not only the emergence and peripheral localization of P_{flaA} -GFP-positive (transmissible) bacteria, but also the efficiency of pathogen vacuole lysis and escape.

Expression of *lqsA* in AYE broth and in *A. castellanii*

Given that *lqsA* and the Lqs system regulate the bistable expression of P_{flaA} , LCV lysis, and spread of *L. pneumophila*, we sought to analyze the expression of *lqsA* and its role for LCV lysis upon over-expression. *Legionella pneumophila* JR32, $\Delta lqsA$, or $\Delta lqsR$ harboring a P_{lqsA} -gfp expression construct were grown in AYE broth, and GFP production was analyzed after 17 h (replicative phase), 21 h (switch to stationary phase), or 25 h (stationary phase), respectively (Fig EV2A). Under these conditions, the P_{lqsA} expression was similar in the three strains tested and strongly induced at the transition from replicative to stationary growth phase (Fig EV2B). In stationary phase, approximately 80% of the bacteria were GFP-positive.

Next, we tested the intracellular expression of P_{lqsA} . We chose 42 h p.i., because at this time point, the intracellular bacteria are in stationary growth phase (Fig 1D) and express P_{flaA} (Fig 1A). *Acanthamoeba castellanii* was infected with *L. pneumophila* JR32, $\Delta lqsA$, $\Delta lqsR$, $\Delta lqsS$, $\Delta lqsT$, or $\Delta lqsS$ - $\Delta lqsT$ harboring the P_{lqsA} -gfp expression construct tested above. However, under these conditions, the intracellular expression of P_{lqsA} was barely detectable (0.5–1% of the bacteria) in all of these strains (Fig EV2C and D, Appendix Fig S6G). Finally, upon infection of *A. castellanii* for 6–48 h with JR32, $\Delta lqsA$, or $\Delta lqsR$, harboring the P_{lqsA} -gfp construct, no P_{lqsA} expression was detectable beyond 6 h (Fig EV2E). At the earliest time point (6 h p.i.), most bacteria were positive for P_{lqsA} -gfp, in agreement with the features of the stationary phase strains used as the infection input (Fig EV2A and B), and similar to what we previously observed for P_{ralF} -gfp and P_{sidC} -gfp (Fig 1B and C). Taken together, P_{lqsA} expression is detected upon growth of *L. pneumophila* wild-type and *lqs* mutant strains in AYE broth, but not intracellularly in *A. castellanii*.

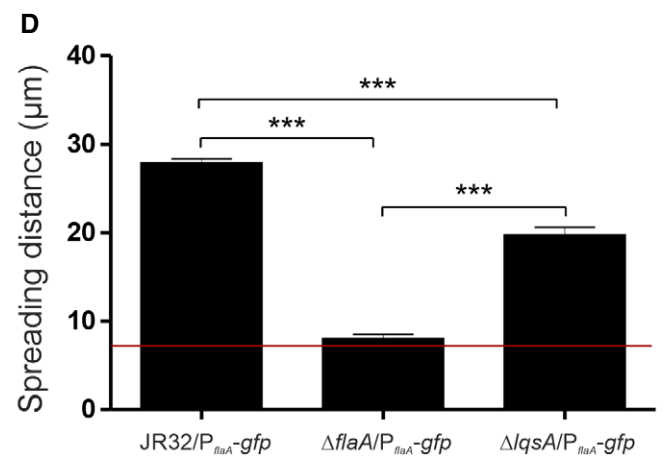
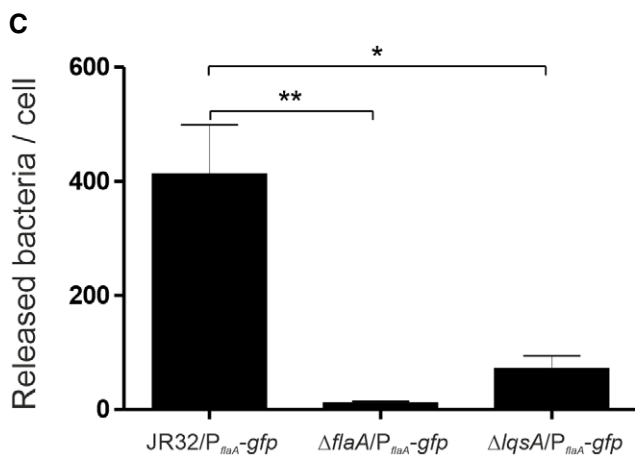
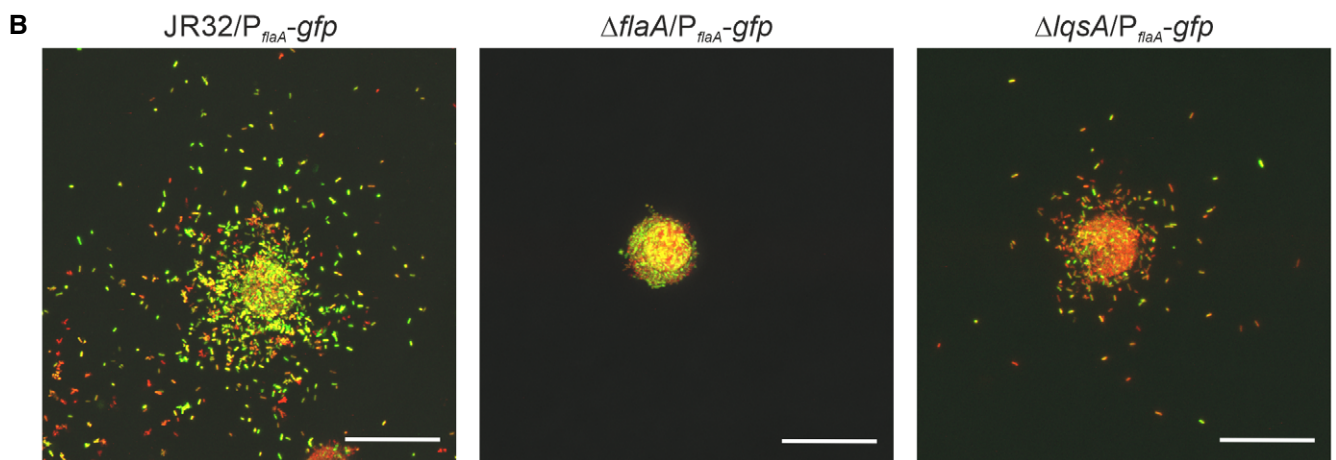
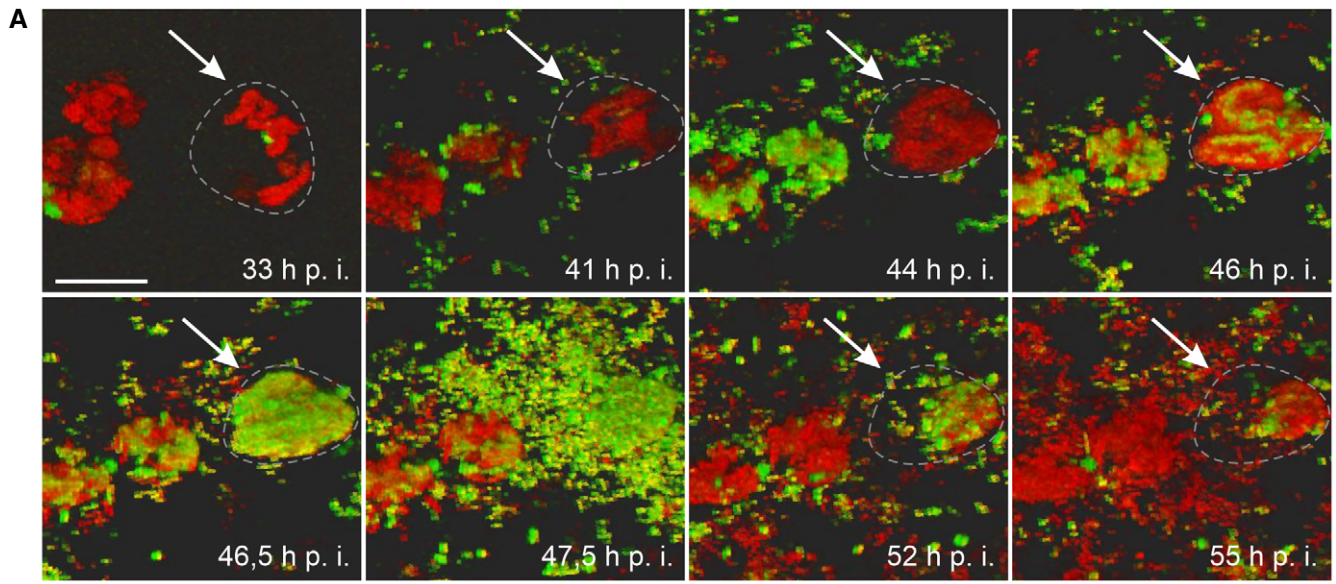


Figure 4.

Figure 4. Spread of *Legionella pneumophila* from lysed *Acanthamoeba castellanii*.

- A Time lapse microscopy of *A. castellanii* infected with P_{flaA} -GFP-producing *L. pneumophila*. *Acanthamoeba castellanii* amoebae were infected (MOI 5) with *L. pneumophila* JR32 (P_{tac} -mCherry- P_{flaA} -gfp) and embedded in 0.5% agarose/PYG medium. Approximately 46 h post-infection, GFP-positive (motile) bacteria emerged in the mCherry-positive intracellular cluster, which within 1.5 h covered the bacterial cluster and spread from the bursting amoeba. At 55 h p.i., primarily mCherry-positive/GFP-negative (non-motile) *L. pneumophila* remained clustered. Scale bar: 10 μ m.
- B *Legionella pneumophila* bacteria lacking *flaA* or *lqsA* are impaired for spreading from amoebae. *Acanthamoeba castellanii* amoebae were infected (MOI 5, 52 h) with *L. pneumophila* JR32, Δ *flaA*, or Δ *lqsA* harboring P_{tac} -mCherry- P_{flaA} -gfp and embedded in 0.5% agarose/PYG medium. The fluorescence images are representative for the *L. pneumophila* strains indicated: JR32 ($n = 25$), Δ *flaA* ($n = 13$), or Δ *lqsA* ($n = 19$). Scale bars: 20 μ m.
- C, D Histograms of the (C) number and (D) spreading distance of *L. pneumophila* released from infected amoebae. Spreading was quantified using the Imaris software ("surface" tool). One mask covered the heavily infected amoebae (center: $x, y, z = 0$), and another mask covered each single bacterium outside the infected host cell. The total number of released bacteria were for JR32 ($n = 1,240$), Δ *flaA* ($n = 33$), and Δ *lqsA* ($n = 214$). The distance of each bacterium to the center was quantified by vector calculations. The red line marks the approximate cell diameter (5 μ m). Data shown are means and SEM of four infected amoebae from one biological replicate (two-tailed Student's *t*-test; * $P < 0.05$, ** $P < 0.01$, and *** $P < 0.001$).

***Legionella pneumophila* phospholipases A and C promote LCV rupture and bacterial escape**

To further assess the mechanism of LCV escape, we tested the role of *L. pneumophila* phospholipases for this process. To this end, LCV escape of wild-type *L. pneumophila* (strain JR32 or Corby) was compared with triple mutant strains deleted for phospholipases. JR32 Δ *plcABC* lacks the Icm/Dot-secreted PlcC (CegC1/Lpg0012) and the type II-secreted PlcA and PlcB (Heidman *et al.*, 2009; Aurass *et al.*, 2013), and Corby Δ *plaACD* lacks the three GDSL phospholipase A family members PlaA, PlaC, and PlaD, where PlaA and PlaC are type II-secreted, and PlaA has been shown to promote LCV lysis in the absence of the effector SdhA (Creasey & Isberg, 2012; Lang *et al.*, 2017). *Dictyostelium discoideum* producing the LCV/PtdIns(4)*P* marker P4C-GFP was infected with these *L. pneumophila* strains for 48 h, and the amoebae harboring cytosolic bacteria were quantified by anti-ubiquitin staining and LCV membrane rupture (Fig 6A). Using this dual labeling approach, LCV lysis (loss of P4C-GFP staining) was inversely correlated with ubiquitination of the bacteria. Under the conditions used, ca. 23% of the amoebae infected with a parental *L. pneumophila* strain harbored intact LCV, compared to ca. 30% of the amoebae infected with the Δ *plcABC* or the Δ *plaACD* triple phospholipase mutants (Fig 6B). Showing an analogous (but inverse) pattern, 2–3 times less amoebae infected with a triple phospholipase mutant (Δ *plcABC*, Δ *plaACD*) harbored ubiquitinated bacteria as compared to the corresponding parental *L. pneumophila* strain (Fig 6C).

As a control, we quantified by flow cytometry the fraction of P_{flaA} -GFP-positive bacteria in the phospholipase triple mutant strains and compared the size of this subpopulation to the corresponding parental strains (Fig 6D, Appendix Fig S6F). The percentage of P_{flaA} -GFP-positive bacteria was similar for *L. pneumophila* strain JR32 and Δ *plcABC*, as well as for strain Corby and Δ *plaACD*, indicating that the phospholipase triple mutants produced P_{flaA} -GFP to the same extent as the isogenic parental strains. In summary, these findings reveal that type IV-translocated as well as type II-secreted *L. pneumophila* phospholipases A and C promote the LCV escape of the motile *L. pneumophila* subpopulation.

In order to test whether the overexpression of *lqsA* has an effect on LCV lysis, we used a plasmid constitutively producing LqsA under control of its own promoter (P_{lqsA}). Upon transformation of *L. pneumophila* Δ *lqsA* or avirulent Δ *icmT* with this construct, the strains inhibit the migration of eukaryotic cells and thus indeed overproduce LqsA (and consequently, LAI-1) (Tiaden *et al.*, 2010b;

Simon *et al.*, 2015). We infected *D. discoideum* producing the LCV/PtdIns(4)*P* probe P4C-mCherry with *L. pneumophila* wild-type strains (JR32, Corby) or phospholipase triple mutants (Δ *plcABC*, Δ *plaACD*) constitutively producing GFP (Fig EV3A and B) or GFP and LqsA under control of its promoter (Fig EV3C and D). While the differences in LCV lysis between the parental strains and the triple phospholipase mutants were similar as documented above (Fig 6), there was no effect of LqsA overproduction on LCV lysis (Fig EV3). This finding is in agreement with the apparent lack of intracellular *lqsA* expression in *A. castellanii* (Fig EV2C–E). Taken together, the phospholipases tested indeed promote LCV lysis by *L. pneumophila*, but the process is apparently not affected by *lqsA* overexpression.

Discussion

Genetically identical bacterial populations show phenotypic heterogeneity, thereby adopting a “bet-hedging” and/or “division of labor” survival strategy to optimally cope with fluctuating environmental conditions (Ackermann, 2015; Grimbergen *et al.*, 2015; Schröter & Dersch, 2019). In this study, we show on a single-cell level that late during infection, a subpopulation of transmissible (virulent and motile) *L. pneumophila* emerges at the LCV periphery (Fig 1). These bacteria selectively spearhead the exit from the pathogen vacuole, host cell rupture, and spread to the environment (Figs 3 and 4). The kinetics of LCV and plasma membrane lysis are fast (minutes, if not seconds), and the stay of *L. pneumophila* in the cytosol is short (minutes), so that very likely no further bacterial replication takes place in the host cell cytosol.

On a population level, the *flaA* gene and other flagellar genes are massively upregulated in stationary growth phase (Brüggemann *et al.*, 2006; Jules & Buchrieser, 2007), in response to an increase in the concentration of the “stringent response” second messenger ppGpp (Hammer & Swanson, 1999; Dalebroux *et al.*, 2010). On a single-cell level, the bistable expression of P_{flaA} and as a consequence bacterial motility is initiated only late during infection (approximately 48 h p.i.), when intracellular bacterial replication has already slowed down, if not ceased (Fig 1). The occurrence of functionally different subpopulations at this late time point adds an intriguing aspect to the long-standing concept of *L. pneumophila* adopting a bi-phasic (replicative/transmissible) life style (Molofsky & Swanson, 2004). Accordingly, in stationary growth phase, *L. pneumophila* is not only virulent, but diverges further into motile and non-motile subpopulations.

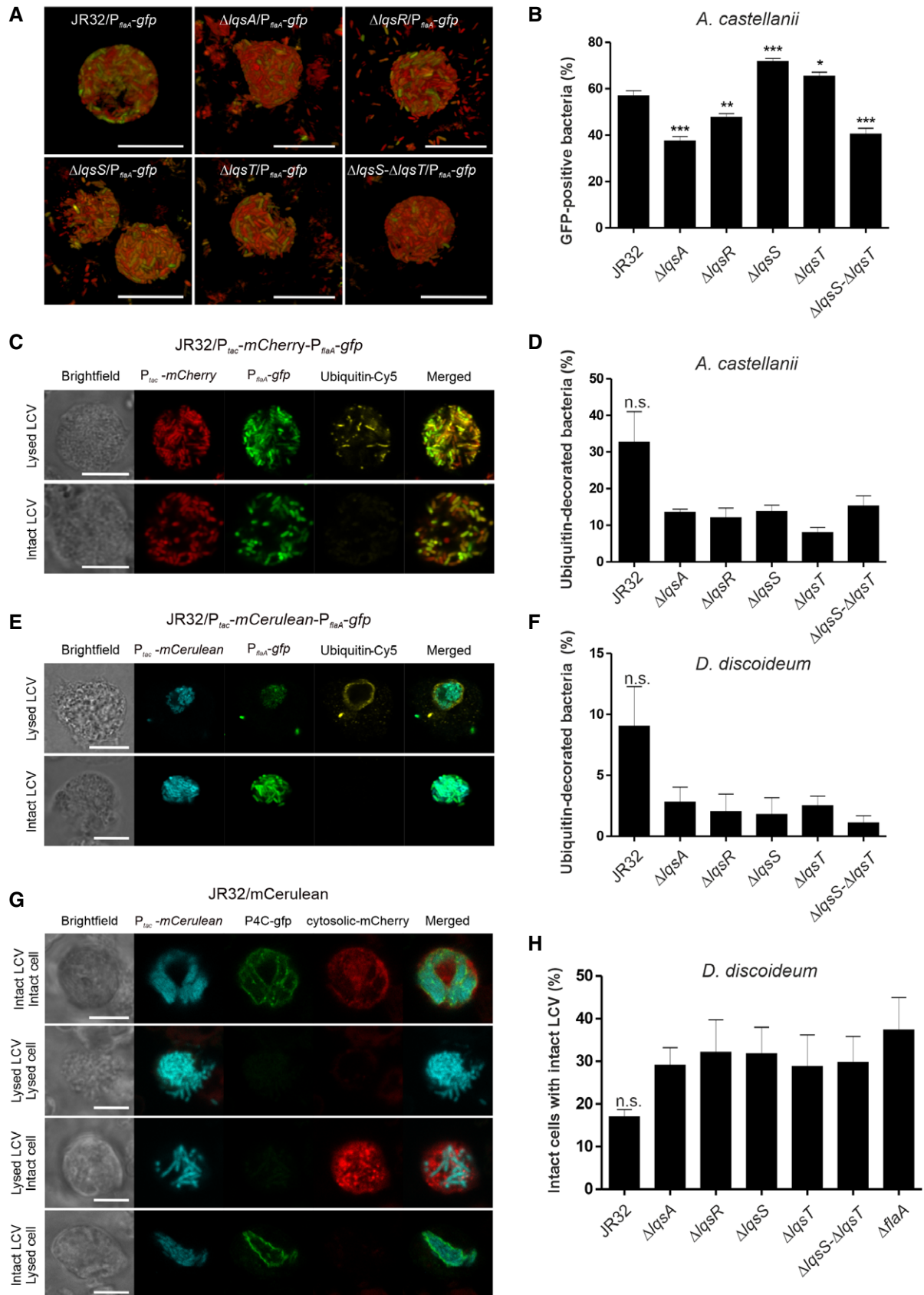


Figure 5.

Figure 5. The Lqs system controls the emergence of a peripheral P_{flaA} -GFP-positive *Legionella pneumophila* population.

- A, B Role of the Lqs system for P_{flaA} expression in intracellular *L. pneumophila*. *Acanthamoeba castellanii* was infected (MOI 5, 48 h) with *L. pneumophila* JR32, $\Delta lqsA$, $\Delta lqsR$, $\Delta lqsS$, $\Delta lqsT$, or $\Delta lqsS$ - $\Delta lqsT$ harboring P_{tac} -mCherry- P_{flaA} -gfp, and (A) fixed and analyzed by confocal microscopy (representative 3D reconstructions, scale bars: 10 μ m), or (B) lysed, fixed, and analyzed by flow cytometry.
- C–F Role of the Lqs system for LCV escape and cytosolic localization of *L. pneumophila*. (C, D) *Acanthamoeba castellanii* or (E, F) *Dictyostelium discoideum* was infected (MOI 5, 48 h) with *L. pneumophila* JR32, $\Delta lqsA$, $\Delta lqsR$, $\Delta lqsS$, $\Delta lqsT$, or $\Delta lqsS$ - $\Delta lqsT$ harboring P_{tac} -mCherry- P_{flaA} -gfp, fixed, and treated with an anti-ubiquitin antibody. Amoebae containing bacteria decorated with ubiquitin were quantified by confocal microscopy. Representative images of (C) *A. castellanii* (scale bars: 10 μ m) or (E) *D. discoideum* (scale bars: 5 μ m) infected with *L. pneumophila* JR32 escaping or not from the LCV are shown. The percentage of amoebae containing ubiquitinated bacteria was quantified by counting the total number of infected cells and the number of ubiquitinated cells: (D) JR32: $n = 482$; $\Delta lqsA$: $n = 834$; $\Delta lqsR$: $n = 572$; $\Delta lqsS$: $n = 729$; $\Delta lqsT$: $n = 1,469$; $\Delta lqsS$ - $\Delta lqsT$: $n = 693$; (F): JR32: $n = 136$; $\Delta lqsA$: $n = 201$; $\Delta lqsR$: $n = 303$; $\Delta lqsS$: $n = 183$; $\Delta lqsT$: $n = 534$; $\Delta lqsS$ - $\Delta lqsT$: $n = 180$.
- G, H *Dictyostelium discoideum* producing the LCV/PtdIns(4)P probe P4C-GFP and cytosolic mCherry was infected (MOI 5, 48 h) with *L. pneumophila* JR32, $\Delta lqsA$, $\Delta lqsR$, $\Delta lqsS$, $\Delta lqsT$, $\Delta lqsS$ - $\Delta lqsT$, or $\Delta flaA$ harboring P_{tac} -mCherry. Representative images of (G) *D. discoideum* infected with *L. pneumophila* JR32 in intact cells with intact LCV (18.5%), lysed cells and lysed LCVs (60.2%), intact cells with intact LCVs (15.5%), and lysed cells with intact LCVs (5.8%) are shown (scale bars: 5 μ m). (H) The percentage of amoebae with intact LCVs was quantified by counting the total number of infected cells and the number of cells with intact LCV membrane: JR32: $n = 426$; $\Delta lqsA$: $n = 468$; $\Delta lqsR$: $n = 344$; $\Delta lqsS$: $n = 325$; $\Delta lqsT$: $n = 287$; $\Delta lqsS$ - $\Delta lqsT$: $n = 289$; $\Delta flaA$: $n = 248$.
- Data information: Data shown (B, D, F, H) are means and SEM from three biological replicates, (B) done in technical triplicate each (two-tailed Student's *t*-test; * $P < 0.05$, ** $P < 0.01$, *** $P < 0.001$, or not significant, n.s.).

While the P_{flaA} -GFP-positive, peripheral *L. pneumophila* subpopulation selectively escapes the LCV and the host cell, the P_{flaA} -GFP-negative interior subpopulation remains clustered amidst the host cell debris and is apparently left behind by the motile, spreading bacteria (Fig 4). Hence, the P_{flaA} -GFP-positive and P_{flaA} -GFP-negative subpopulations are spatially organized and adopt distinct functions. The P_{flaA} -GFP-positive motile bacteria spread from the destroyed amoebae, are likely P_{ralF} - and P_{sidC} -GFP-positive (virulent), and can readily infect other host cells in a distance. In turn, the P_{flaA} -GFP-negative non-motile population, a fraction of which is also P_{ralF} - and P_{sidC} -GFP-positive (Fig 1B and C), might be well suited to locally infect “grazing” amoebae and/or might be physiologically better equipped to adhere to and thrive in a comparably rich (biofilm) environment. Overall, this phenotypic heterogeneity likely represents a typical bet-hedging survival strategy, where a bacterial subpopulation prepares itself to colonize new, nutrient-rich niches, while another subpopulation stays behind in what at some point was (and might still be or become again) a growth-permissive niche.

Different functions of the P_{flaA} -GFP-positive and the P_{flaA} -GFP-negative *L. pneumophila* subpopulations are also supported by the comparative proteomics analysis, which revealed distinct proteomes (Fig 2, Appendix Fig S3). Only the P_{flaA} -GFP-positive subpopulation produced proteins implicated in flagellum production (Fig 2B). In contrast, the P_{flaA} -GFP-negative subpopulation upregulated the production of proteins implicated in cell division and replication (Fig 2C). Even though these bacteria appear to grow only slowly or not at all at the end of an infection (Fig 1), the production of cell division and replication proteins might allow for a more rapid growth resumption, once the nutritional conditions become more favorable. Such a configuration is in agreement with the concept of adopting a bet-hedging strategy. Thus, intracellularly growing *L. pneumophila* might broaden their response repertoire to optimally meet different intra- and extracellular conditions before killing and escaping from the host cell.

Another reason underlying the occurrence of P_{flaA} -GFP-positive and P_{flaA} -GFP-negative *L. pneumophila* subpopulations might be that only a fraction of the population needs to engage in the bioenergetically costly production of the flagellum. The monotruncated *L. pneumophila* flagellum is a complex multisubunit structure, the production of which is tightly regulated by nutrient limitation in the

stationary growth phase and quorum sensing at high cell density (Albert-Weissenberger *et al*, 2010; Schell *et al*, 2016a; Appelt & Heuner, 2017). Moreover, it appears that the P_{flaA} -GFP-positive subpopulation “paves the way” for P_{flaA} -GFP-negative bacteria during LCV exit and host cell lysis (Fig 3). In light of these considerations, phenotypic heterogeneity of *L. pneumophila* at late stages of infection might also be regarded as a division of labor strategy (Ackermann, 2015; Schröter & Dersch, 2019).

Intriguingly, both the P_{flaA} -GFP-positive and the P_{flaA} -GFP-negative *L. pneumophila* subpopulations produced the Icm/Dot T4SS and some well-known translocated effectors such as SidC (Luo & Isberg, 2004; Weber *et al*, 2006; Ragaz *et al*, 2008), suggesting that both subpopulations are virulent (Fig 2). In agreement with this notion, infection experiments with FACS-sorted P_{flaA} -GFP-positive and P_{flaA} -GFP-negative populations did not demonstrate significant differences regarding the virulence of the subpopulations (Appendix Fig S3E). *Legionella pneumophila* is most virulent in the stationary growth phase (Molofsky & Swanson, 2004). However, recent proteomics studies revealed that some effector proteins are produced in the exponential growth phase, while others are produced in the stationary growth phase (Aurass *et al*, 2016). The effectors RalF, SidC, and LegC8 are produced in the post-exponential growth phase in broth (Nagai *et al*, 2002; Luo & Isberg, 2004; Aurass *et al*, 2016). Noteworthy, under the conditions used here, LegC8 is preferentially produced in the P_{flaA} -GFP-negative (non-growing) *L. pneumophila* subpopulation in amoebae (Fig 2E). This raises the intriguing possibility that distinct intracellular *L. pneumophila* subpopulations produce different effector protein profiles, which might have specific functions at different steps of the infection process. Accordingly, the production and secretion of specific effectors might reflect distinct temporal or spatial aspects of *L. pneumophila* virulence.

On a population level, the expression of flagellar genes and the production of flagellin as well as bacterial motility are regulated by the quorum sensing response regulator LqsR (Tiaden *et al*, 2007; Hochstrasser *et al*, 2019) and the signaling compound LAI-1 (Schell *et al*, 2016b). On a single-cell level, the emergence of P_{flaA} -GFP-positive, transmissible *L. pneumophila* at the LCV boundary is also controlled by the Lqs quorum sensing system (Figs 4B–D and 5). While only some *L. pneumophila* strains lacking Lqs components

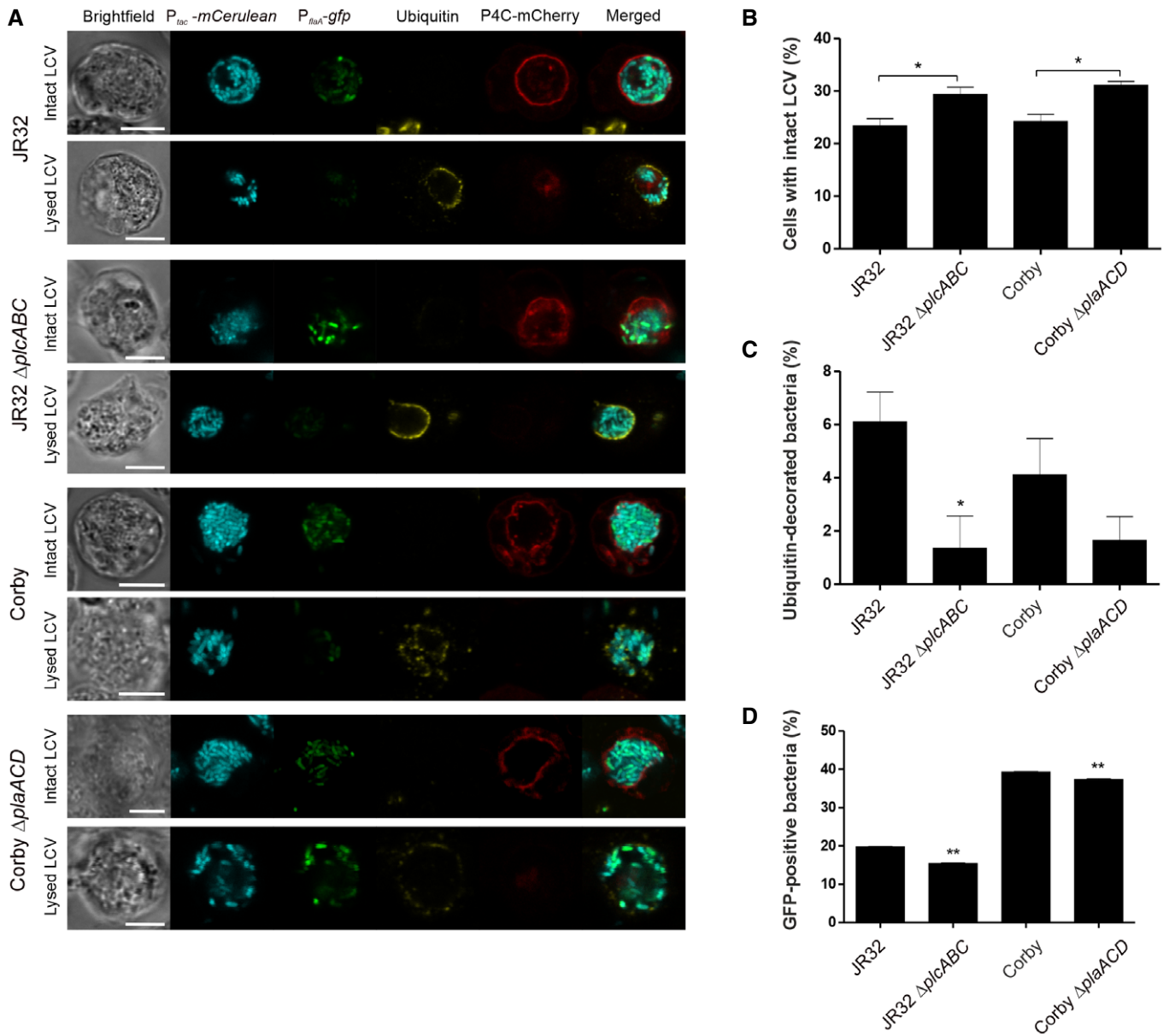


Figure 6. *Legionella pneumophila* phospholipases A and C promote LCV exit.

A–D *Dictyostelium discoideum* producing the LCV/PtdIns(4)P probe P4C-mCherry was infected (MOI 5, 48 h) with *L. pneumophila* wild-type strains (JR32, Corby), or phospholipase triple mutants ($\Delta plcABC$, $\Delta plaACD$) harboring the P_{tac} -mCerulean- P_{flaA} -gfp reporter construct, and (A–C) fixed and treated with an anti-ubiquitin antibody, or (D) lysed, fixed, and analyzed by flow cytometry. LCV escape and cytosolic localization of the bacteria was assessed by confocal microscopy through quantification of amoeba containing intact, P4C-mCherry-positive LCVs or ubiquitin-decorated, cytosolic bacteria. (A) Representative images of amoebae harboring *L. pneumophila* confined within LCVs or released from the LCV to the cytosol are shown (scale bars: 5 μ m). (B) The percentage of *D. discoideum* with intact LCVs was assessed for the following number of cells: JR32, $n = 132$; JR32 $\Delta plcABC$, $n = 606$; Corby, $n = 265$; Corby $\Delta plaACD$, $n = 357$. (C) The percentage of *D. discoideum* harboring ubiquitinated *L. pneumophila* was assessed for the following number of cells: JR32, $n = 100$; JR32 $\Delta plcABC$, $n = 602$; Corby, $n = 281$; Corby $\Delta plaACD$, $n = 389$. (D) Quantification of GFP-positive bacteria of the *L. pneumophila* strains by flow cytometry and FlowJo software. Data shown are means and SEM from (B, C) three biological replicates and (D) a technical triplicate (two-tailed Student's t -test; * $P < 0.05$ and ** $P < 0.01$).

($\Delta lqsA$, $\Delta lqsR$, $\Delta lqsS$ - $\Delta lqsT$) produced fewer P_{flaA} -GFP-positive *L. pneumophila* in the LCV (Fig 5A and B), all *lqs* mutant strains were impaired for LCV escape (Fig 5C–H). A possible explanation for this observation is that, even though P_{flaA} expression serves as a proxy for the transmissible (motile and virulent) phase of *L. pneumophila*, the escape from the LCV is a more complex process very

likely requiring a number of different type IV- and/or type II-secreted virulence factors. Hence, the more pleiotropic role of the Lqs system regarding LCV escape is reflected in more severe phenotypes of the corresponding deletion mutants.

Time lapse microscopy analysis of intravacuolar *L. pneumophila* revealed that only a few individuals initially engaged in the

phenotypic conversion to the P_{flaA} -GFP-positive, transmissive phase (Figs 1A and 4A, Movie EV9). Phenotypic conversion propagated to neighboring cells and was restricted to peripheral individuals. The mechanism driving spatial segregation and growth of the peripheral subpopulation is unknown, but likely involves cell-to-cell communication through the Lqs system (Fig 5). Spatially correlated gene expression in bacterial groups might be explained by spatial gradients, cell–cell interactions, and/or the cell lineage history (van Vliet et al, 2018). Intriguingly, *L. pneumophila* also engages in spatially controlled phenotypic conversion in microcolonies grown on abiotic surfaces (Personnic et al, 2021).

The Lqs system functions as a master regulator of *L. pneumophila* phenotypic heterogeneity under different environmental circumstances, such as amoebae and biofilms. Within amoebae, the Lqs system positively regulates the emergence of replicating and non-replicating *L. pneumophila* subpopulations of similar size at early time points during infection (< 24 h) (Personnic et al, 2019b). The process is reversible and yields non-growing bacteria, which are metabolically active and viable, display increased antibiotic tolerance, and show high virulence. Hence, the non-growers are virulent persisters. In the absence of components of the Lqs system, the non-growing intracellular population is smaller. Moreover, this study revealed that at late stages of infection (> 42–48 h), the Lqs system also regulates the emergence of intracellular transmissive *L. pneumophila* (Fig 5), some of which are likely persisters (Appendix Fig S3F).

In biofilms and microcolonies, the Lqs system also regulates the ratio of growing and non-growing *L. pneumophila* populations (Personnic et al, 2021). Non-growing sessile bacteria are metabolically active, express virulence genes, and show tolerance toward antibiotics. Thus, similar to intracellular *L. pneumophila*, the sessile non-growers are virulent persisters. The Lqs system controls not only the ratio between growing and non-growing sessile populations, but also the frequency of growth resumption (“resuscitation”) and microcolony formation of individual bacteria. However, in the absence of Lqs components, the non-growing population in biofilms is larger. In summary, at early and late stages of amoeba infection, the Lqs system positively regulates the emergence of virulent and motile persisters (Personnic et al, 2019b) (Fig 5), while in biofilms, the Lqs system negatively regulates the occurrence of non-growing bacteria (Personnic et al, 2021).

The Lqs system not only promotes P_{flaA} -GFP production and motility of intravacuolar *L. pneumophila* (Figs 1, 4B–D and 5), but also cross-talks with the cyclic-di-GMP signaling network through the pleiotropic transcription factor LvbR (Hochstrasser et al, 2019; Hochstrasser & Hilbi, 2020). The sensor kinase LqsS negatively regulates LvbR, which promotes the production of a guanylate cyclase, and hence regulates cyclic-di-GMP metabolism (Hochstrasser et al, 2019; Hochstrasser & Hilbi, 2020). Remarkably, the heterogeneous induction of the flagellar machinery in other bacterial species such as *Caulobacter crescentus* or *Pseudomonas aeruginosa* has been linked to cell-to-cell heterogeneity in c-di-GMP concentrations resulting from an asymmetrical cell division (Kulasekara et al, 2013; Laventie et al, 2019). Spatially organized cyclic-di-GMP gradients might also underlie the flagellum production in *L. pneumophila*. Interestingly, LvbR is a negative regulator of the nitric oxide (NO) sensor Hnox-1, and therefore, exogenous NO signaling might be a potential environmental cue triggering phenotypic heterogeneity and

the peripheral emergence of the non-growing/transmissive subpopulation of intracellular *L. pneumophila*.

Legionella pneumophila flagellin promotes LCV lysis (Fig 5H), but is not essential for LCV rupture and host cell lysis (Fig 4B–D). Furthermore, the Icm/Dot T4SS has also been implicated in pore formation-mediated egress of the bacteria from host cells (Molmeret et al, 2002a; Molmeret et al, 2002b), but effector proteins promoting LCV and/or host cell exit are not known. The proteomes of P_{flaA} -GFP-positive and P_{flaA} -GFP-negative *L. pneumophila* subpopulations revealed an enrichment of flagellar proteins or cell division proteins, respectively (Fig 2), but no obvious candidates for *L. pneumophila* factors implicated in compartment escape were identified.

A triple mutant strain lacking the Icm/Dot-secreted phospholipase C, PlcC (CegC1/Lpg0012) and type II-secreted PlcA and PlcB (Aurass et al, 2013), and a triple mutant strain lacking the type II-secreted GDSL lipase family members PlaA and PlaC, as well as PlaD (Lang et al, 2017), were impaired for LCV rupture in *D. discoideum* (Fig 6). These results indicate that phospholipases A and C are involved in LCV and host plasma membrane lysis, and they are in agreement with a role for PlaA for pathogen vacuole disruption and host cell death in the absence of the Icm/Dot-translocated effector SdhA (Creasey & Isberg, 2012). Intracellular overexpression of *lqsA* had no effect on phospholipase-mediated LCV lysis (Fig EV3). However, at this point it is unclear, under which conditions and to what extent *lqsA* is expressed intracellularly (Fig EV2).

Indeed, the *lqsA* gene does not seem to be expressed intracellularly in *A. castellanii* (Fig EV2) and, accordingly, does not seem to affect phospholipase-dependent LCV lysis (Fig EV3). However, we provide strong evidence that components of the Lqs system modulate the emergence of P_{flaA} -positive *L. pneumophila* at 42 h p.i. (Appendix Fig S6B and C), as well as at 48 h p.i. (Fig 5A and B). A rather trivial reason for these observations might be that the P_{lqsA} -*gfp* reporter used in these experiments is not sensitive enough and *lqsA* is expressed below the limit of detection of this reporter. More intriguingly, *lqsA* expression might indeed be negatively regulated (and thus not be required) intracellularly, while being positively regulated upon growth in AYE broth (Fig EV2A and B). In agreement with this notion, the $\Delta lqsA$ mutant strain has only a weak virulence phenotype (Tiaden et al, 2010b). Moreover, it has been long known that growth of *L. pneumophila* in broth is only a proxy for the processes going on in amoebae, as bacteria grown in broth to stationary phase are less virulent compared to bacteria emerging from amoebae (Cirillo et al, 1994).

Importantly, not only the (concentration-dependent) presence of LAI-1, but also its absence has major regulatory implications. In the absence of the autoinducer, the LAI-1-responsive sensor histidine kinases LqsS and LqsT are preferentially phosphorylated, which in turn leads to LqsR phosphorylation and dimerization (Schell et al, 2014; Schell et al, 2016b). Hence, the role of quorum sensing (and LAI-1 concentration) might indeed be inversely correlated to the extent of the vacuolar phenotypic heterogeneity observed and the spatio-temporal distinct emergence of a transmissive *L. pneumophila* subpopulation.

Legionella pneumophila flagellin represents a conserved “pathogen-associated molecular pattern” (PAMP) and as such is sensed by metazoan phagocytes (Schell et al, 2016a; Mascarenhas & Zamboni, 2017). Flagellin is recognized by the mammalian innate

immune sensor NAIP5 (Birc1e) (Molofsky *et al*, 2006; Ren *et al*, 2006; Zamboni *et al*, 2006; Lightfield *et al*, 2008), which upon binding to and activation of the NLRC4 (IpaF) inflammasome proteolytically activates the protease caspase-1 (Amer *et al*, 2006; Silveira & Zamboni, 2010; Kofoed & Vance, 2011; Pereira *et al*, 2011a; Pereira *et al*, 2011b). The activation of the inflammasome and caspase-1 leads to pore formation and pyroptosis, thus destroying and removing the cellular replicative niche of *L. pneumophila*. Given that *L. pneumophila* co-evolved mainly if not exclusively in association with environmental protozoa, the recognition of flagellin might not be relevant or be different for protozoa (which lack inflammasomes and caspases). However, the detection and response to flagellin is clearly relevant for pathogenesis in humans (Newton *et al*, 2010; Simon & Hilbi, 2015; Mascarenhas & Zamboni, 2017). Accordingly, the P_{flaA} -GFP-positive (flagellated, motile and virulent) as well as the P_{flaA} -GFP-negative (non-flagellated, non-motile and virulent) *L. pneumophila* populations likely contribute to Legionnaires' disease onset and/or progression.

In summary, in the current study we characterized a P_{flaA} -positive transmissible *L. pneumophila* subpopulation, which is regulated by the Lqs system, preferentially emerges at the LCV periphery, and promotes the exit of *L. pneumophila* from the pathogen vacuole and spread from the ruptured host cell. These findings pave the way to identify and characterize the molecular “executors” of Lqs-dependent phenotypic heterogeneity of *L. pneumophila*, such as the bacterial effectors implicated in LCV exit and host cell lysis.

Materials and Methods

Bacteria, cells, and infection conditions

The bacterial strains used are listed in Appendix Table S1. *Legionella pneumophila* strains were grown for 3 days on charcoal yeast extract (CYE) agar plates, with or without chloramphenicol (Cam; 5 µg/ml) at 37°C. Bacterial colonies were used to inoculate liquid cultures in ACES yeast extract (AYE) medium with or without Cam (5 µg/ml) with a starting concentration of an OD₆₀₀ of 0.1. *Escherichia coli* TOP10 was cultured in LB broth, and antibiotics were added as required at the following concentrations: Cam (30 µg/ml) or ampicillin (Amp; 100 µg/ml).

Acanthamoeba castellanii amoebae (ATCC 30234, laboratory collection) were grown in proteose, yeast extract, glucose (PYG) medium at 23°C. *Dictyostelium discoideum* amoebae (Ax3, laboratory collection) were grown in HL5 medium (ForMedium) at 23°C and transfected by electroporation with a Gene Pulser Xcell (Bio-Rad) device as described (Weber *et al*, 2014). After 24 h, transfectants were selected and maintained in HL5 medium containing hygromycin (50 µg/ml) and/or geneticin (G418, 20 µg/ml). Murine macrophage-like RAW 264.7 cells (ATCC TIB-71, laboratory collection) were cultivated in RPMI 1640 medium (Life Technologies) supplemented with 10% heat-inactivated fetal calf serum (FCS; Life Technologies) and 1% glutamine (Life Technologies) at 37°C with 5% CO₂ in a humidified atmosphere. The amoebae and macrophages were grown in T75 flasks and split every 2nd or 3rd day.

For infections, *L. pneumophila* was inoculated at an OD₆₀₀ 0.1 in AYE medium and grown on a wheel at 37°C for 21–22 h to early stationary phase (OD₆₀₀ ca. 5.0, ~2 × 10⁹ bacteria/ml). The

cultures were routinely checked under the microscope (motile, non-filamentous bacteria). Cam (5 µg/ml) was added as required. Cultures were diluted to the desired density, and the infection of cells was synchronized by centrifugation (450 g, 10 min; room temperature, RT). After 1–2 h, the infected cells were washed 4 times with PYG (*A. castellanii*), HL5 (*D. discoideum*) or RPMI 1640/10% FCS (RAW 264.7 macrophages) stored at RT or warmed up to 37°C, respectively, and further incubated at the temperature and for the time indicated. Depending on the experimental setup, the infected cells were imaged live, lysed with 0.1% Triton X-100, and/or fixed with 4% paraformaldehyde (PFA).

Molecular biology and plasmid construction

The plasmids used in this study are listed in Appendix Table S1. Cloning was performed using standard protocols, plasmids were isolated by using commercially available kits from Qiagen or Macherey-Nagel, DNA fragments were amplified using Phusion High Fidelity DNA polymerase, and the primers are listed in Appendix Table S2. For Gibson assembly, the NEBuilder HiFi DNA assembly kit was used. All constructs were verified by DNA sequencing.

The plasmids pBI001 and pSV010 harboring transcriptional fusions of P_{fleQ} -*mCherry*- P_{flaA} -*gfp* or P_{legC8} -*mCherry*- P_{flaA} -*gfp* were constructed using the primer pair oBI020/oBI025 or oSV150/oSV151 and genomic DNA from the *L. pneumophila* strain JR32 as template. The PCR fragments were cloned into the *ApaI* and *SacI* sites of pSN7 (Personnic *et al*, 2019b), thus replacing P_{tac} -*mCherry* with P_{fleQ} -*mCherry* or P_{legC8} -*mCherry*, respectively. Plasmid pRH032 harboring a transcriptional P_{ralF} -*gfp* fusion and pRH035 harboring a transcriptional P_{sidC} -*gfp* fusion were constructed by exchanging P_{flaA} in pCM009 (Schell *et al*, 2016b). To this end, P_{ralF} (putative *ralF/lpg1950* promoter: 515 bp) or P_{sidC} (putative *sidC/lpg2511* promoter: 507 bp) was amplified by PCR using the primers oRH130/oRH131 or oRH172/oRH173 and genomic DNA as template, and the PCR product was cloned into the *SacI* and *XbaI* sites of pCM009. Plasmid pSB002 harboring a transcriptional P_{tac} -*mCherry*- P_{ralF} -*gfp* (*GFP_{ASV}*) fusion was constructed by replacing P_{flaA} -*gfp* (*GFP_{AAV}*) in pSN7. To this end, P_{ralF} -*gfp* (*GFP_{ASV}*) was amplified by PCR using the primers oRH180/oRH181 and pRH032 as template, and the PCR product was cloned into the *BamHI* and *XhoI* sites of pSN7.

The plasmid pKA059 harboring a transcriptional P_{tac} -*mCerulean*- P_{flaA} -*gfp* fusion was constructed by replacing *mCherry* with *mCerulean* in pSN7 (Personnic *et al*, 2019b). To this end, pSN7 (P_{tac} -*mCherry*- P_{flaA} -*gfp*) excluding *mCherry* was amplified with the primers oKA136 and oKA137 using Q5 Hot Start High Fidelity DNA polymerase (with Q5 High GC Enhancer added), and *mCerulean* was amplified with the primers oKA124 and oKA125. Short sequences overlapping with pSN7 were fused to *mCerulean* during amplification. Finally, both fragments were assembled using the NEBuilder HiFi DNA assembly kit.

Mass spectrometry-based proteome analysis

To prepare samples for proteomics analysis, approximately 1 × 10⁷ cells were lysed in 100 µl of lysis buffer (1% sodium deoxycholate, 10 mM tris(2-carboxyethyl)phosphine, 100 mM Tris, pH 8.5). 25 µl lysis buffer was added to each sample and incubated (15 min,

95°C). Duplicates were combined, and empty Eppendorf tubes were rinsed with 10 µl lysis buffer each and also combined. The samples were treated with 30 sonication cycles (each 30 s on, 30 s off) using a Bioruptor device (Diagenode). Subsequently, proteins were reduced (10 min, 95°C) and, after cooling to RT, alkylated in 15 mM chloroacetamide (30 min, 37°C). The proteins were digested (overnight, 37°C) using sequencing-grade modified trypsin (1/50, w/w, trypsin/protein; Promega). After digestion, the samples were supplemented with trifluoroacetic acid to a final concentration of 1%. Peptides were cleaned up using PreOmics Cartridges (PreOmics; Martinsried, Germany) following the manufacturers' instructions. After drying the samples under vacuum, the peptides were resuspended in 0.1% aqueous formic acid solution at a concentration of 0.5 mg/ml. 0.5 µg of peptides of each sample was subjected to liquid chromatography (LC)/mass spectrometry (MS) analysis using a dual pressure LTQ-Orbitrap Elite mass spectrometer connected to an electrospray ion source (both Thermo Fisher Scientific), as specified (Ahrné *et al*, 2016) and a custom-made column heater set to 60°C.

Peptide separation was carried out using an EASY nLC-1000 system (Thermo Fisher Scientific) equipped with a RP-HPLC column (75 µm × 30 cm) packed in-house with C₁₈ resin (ReproSil-Pur C18-AQ, 1.9 µm resin; Dr. Maisch GmbH, Ammerbuch-Entringen, Germany) using a linear gradient from 95% solvent A (0.1% formic acid, 99.9% water) and 5% solvent B (80% acetonitrile, 0.1% formic acid, 19.9% water) to 35% solvent B over 50 min to 50% solvent B over 10 min to 95% solvent B over 2 min and 95% solvent B over 18 min at a flow rate of 0.2 µl/min.

The data acquisition mode was set to obtain one high-resolution MS scan in the FT part of the mass spectrometer at a resolution of 240,000 full width at half maximum (at 400 *m/z*, MS1) followed by MS/MS (MS2) scans in the linear ion trap of the 20 most intense MS signals. The charged state screening modus was enabled to exclude unassigned and singly-charged ions, and the dynamic exclusion duration was set to 30 s. The ion accumulation time was set to 300 msec (MS1) and 25 msec (MS2). MS1 and MS2 scans were acquired at a target setting of 1,000,000 ions and 10,000 ions, respectively. The collision energy was set to 35%, and one microscan was acquired for each spectrum.

Label-free peptide quantification was performed as follows: In the LFQ workflow, MS raw files were imported into Progenesis QI (Nonlinear Dynamics, v2.0) and analyzed using the default parameter settings. MS/MS data were exported directly from Progenesis in mgf format and analyzed using Mascot (Matrix Science, version 2.4.1), against a concatenated target-decoy database containing normal and reverse sequences of the predicted Swiss-Prot entries of *L. pneumophila* (ATCC_33152/DSM_7513; www.uniprot.org, release date 9/05/2017), and commonly observed contaminants (in total 10,006 protein sequences) generated using the SequenceReverser tool from the MaxQuant software (Version 1.0.13.13). The Mascot search criteria were set as follows: 10 ppm precursor ion mass tolerance, 0.6 Da fragment ion mass tolerance, full tryptic specificity required (cleavage after lysine or arginine residues unless followed by proline), maximum of three missed cleavages, fixed modifications, carbamidomethylation; variable modification, oxidation (M) and acetyl (protein N-terminus). Results from the database search were imported into Progenesis, and a list with all quantified peptides was exported. The quantitative data were further processed

and statistically analyzed using the SafeQuant software tool (Glatter *et al*, 2012). In brief, the false discovery rate (FDR) of identifications on the peptide and protein level was set to 1% based on the number of decoy hits obtained from reversed protein sequence entries. For quantification, the analysis included global data normalization by equalizing the total peak areas across all LC-MS runs, summation of peak areas per protein and LC-MS/MS run, followed by calculation of protein abundance ratios. Only isoform specific peptide ion signals were considered for quantification. The summarized protein expression values were used for statistical testing of proteins differentially abundant between conditions. Here, empirical Bayes moderated *t*-tests were applied, as implemented in the R/Bioconductor limma package (<http://bioconductor.org/packages/release/bioc/html/limma.html>). The resulting per protein and condition comparison *P*-values were adjusted for multiple testing using the Benjamini–Hochberg method. All results together with protein abundance estimates using the iBAQ approach (Ahrné *et al*, 2013) are reported for every protein in the Dataset EV1.

Confocal microscopy and image processing

Infections were performed in 35-mm microscopy dishes or in 6-well plates, with 1.8×10^6 amoeba per sample. For time points < 24 h, the infected cells in dishes were directly fixed and embedded in a thin layer of agarose in amoebae medium (Personnic *et al*, 2019a). For time points > 24 h, most infected cells in six-well plates had detached (due to the high infection load), and the supernatants were collected in a 2-ml Eppendorf tube, centrifuged, fixed with 4% PFA, and concentrated prior to embedment in 0.5% agarose in PYG medium (eight-well ibidi dish). For DAPI staining, infected *A. castellanii* (MOI 5, up to 48 h) were fixed with 4% PFA, permeabilized with or ice-cold methanol (10 min), washed twice, treated with DAPI in PBS (1 µg/ml; 1 h, RT), washed twice with PBS, pelleted, and resuspended in 30 µl PBS. The concentrated cells were added into an 8-well ibidi dish and embedded in 0.5% agarose in PYG medium.

Live-cell imaging was performed in 35-mm dishes (1.8×10^6 cells) or 8-well ibidi dishes (3×10^5 cells) and infected for 2 h, followed by a wash step and embedment in agarose in PYG medium. The infected cells were incubated for the time indicated at 25°C and imaged by live-cell microscopy. The agarose concentration varied among experiments (0.5–1.0%) to allow different spreading distances during the experiments.

Microscopy was performed using a Leica SP8 X CLSM and Leica LAS X software with the following setup: white light laser, HyD hybrid detectors for each channel (488 nm/561 nm), HC PL APO CS2 63×/1.4 oil objective with Leica Type F immersion oil, pixel size (x: 40–60 nm, y: 40–60 nm, z: 130 nm). Image processing was done with the ImageJ and/or Imaris software (without deconvolution). Fluorescence imaging at a single-cell level was performed under the following conditions: *P_{tac}-mCherry-P_{flaA}-gfp*, *P_{ratF}-gfp* and Timer reporter color ratio (GFP/green, excitation 488 nm, emission 515–545 nm; mCherry/red, excitation 561 nm, emission 600–620 nm), *P_{tac}-mCerulean-P_{flaA}-gfp* (mCerulean, excitation 442 nm, emission 464–483 nm), secondary antibody: goat α-mouse IgG coupled to Cy5 (Cy5, excitation 647 nm, emission 670–695 nm), DAPI (DAPI, excitation 405 nm, emission 457 nm). For real-time microscopy, the images were acquired with a speed of one frame per sec, exported

to ImageJ, and processed with this software as an AVI file with seven frames (TIFF files) per sec (i.e., the live-cell process was sped up seven times).

Escape of *L. pneumophila* from LCVs into the host cell cytosol was analyzed by ubiquitination as described (Koliwer-Brandl *et al*, 2019). Briefly, *D. discoideum* or *A. castellanii* were infected (MOI 5, 48 h) with different *L. pneumophila* strains harboring P_{tac} -mCherry- P_{flaA} -gfp or P_{tac} -mCerulean- P_{flaA} -gfp, fixed with 4% PFA, and permeabilized with PBS/1% BSA/0.1% Triton X-100 (10 min) or ice-cold methanol (10 min), respectively. The fixed cells were blocked with PBS/1% BSA (1 h), washed twice, and treated with a monoclonal anti-ubiquitin antibody (FK2, Enzo), diluted 1:1,000 in PBS/1% BSA (overnight, 4°C), followed by a wash step and addition of the secondary antibody (goat α -mouse IgG Cy5 or goat α -mouse IgG Alexa Fluor 647; Jackson Laboratory) diluted 1:250 in PBS/1% BSA (1.5 h, RT). Finally, the amoebae were washed three times with PBS, pelleted, and resuspended in 30 μ l PBS. The suspension was then added into an 8-well ibidi dish and embedded in 0.5% agarose in PBS.

The spreading distance of *L. pneumophila* was calculated with fluorescence images by using Imaris. To this end, the x , y , and z coordinates of each bacterium were calculated relative to the host cell center defined as $x = 0$, $y = 0$, and $z = 0$. First, a mask was defined, allowing the infected host cell and internalized bacteria to be excluded. A second mask was defined, where single bacteria were selected in the remaining area outside of the first mask. The coordinates of the bacteria residing in mask 2 but not mask 1 were exported to Excel, and the distance from each bacterium to the center was calculated by vector calculations. These data were then transferred to GraphPad Prism, and histograms were constructed.

Fluorescence recovery after photobleaching

For FRAP experiments, *A. castellanii* were infected (MOI 5) with *L. pneumophila* JR32 in 35-mm dishes (ibidi) for 2 h, washed, and embedded in a layer of PYG/0.5% agarose. 47 h p.i., the infected cells were treated with erythromycin (60 μ g/ml) or not and incubated for another hour. Fluorescence acquisition was performed using the confocal microscope Leica SP8 at 63 \times magnification. Photobleaching was set up according to the FRAP-wizard of the Leica user interface on narrowed regions of interest and performed using the FRAP-booster, 100% 488 nm laser intensity for 79 ms and 30 \times iterations.

Flow cytometry analysis and FACS

For flow cytometry, the infected cells were ruptured in lysis buffer (150 mM NaCl, 0.1% Triton X-100; 10 min, RT) and centrifuged (5 min, 2,000 g). The pellets, or bacteria grown in broth, were fixed with 4% PFA (30 min, RT), washed twice in PBS, and analyzed with an LSRFortessa II (BD Biosciences). The gating strategy for bacteria producing Timer or the dual reporter mCherry/GFP (P_{flaA}) is described in Personnic *et al* (2021). The gating strategy for bacteria producing the dual reporter mCerulean/GFP (P_{flaA}) had to be adapted, since the LSRFortessa II does not detect mCerulean. To this end, bacteria producing GFP only (control) and bacteria producing the dual reporter P_{tac} -mCherry- P_{flaA} -gfp were used to gate only for the P_{flaA} -positive population. The control was illuminated with the

488 and V450 laser line (GFP: 550 parameter number volt (PnV), V450: 477 PnV), to check whether the dot plot does not vary and to check for possible cross-talk with the P_{tac} -mCerulean signal. The threshold for FSC and SSC was set to 200, and at least 20,000 events were acquired. Data processing was performed with the FlowJo software.

For cell sorting, *A. castellanii* were seeded into six 10-cm dishes (7.5×10^6 cells/dish), grown overnight and infected with *L. pneumophila* (MOI 5, 2 h), washed, and further incubated for 40 h at 25°C. After 24 h, Amp (100 μ g/ml) was added to remove extracellular bacteria. The cells in the supernatant were collected in a 50-ml tube and centrifuged (10 min, 2,000 g, 4°C). The supernatant was removed, and the cells were resuspended in 40 ml ice-cold lysis buffer (HS-buffer: 20 mM *N*-2-hydroxyethylpiperazine-*N*-2-ethanesulfonic acid, 250 mM sucrose, 0.5 mM ethyleneglycoltetraacetic acid, pH 7.2; containing 5 μ g/ml Cam, 40 μ l Triton X-100, 4 tabs of protease inhibitor) and incubated until the liquid was no longer turbid (12 min, 30°C). The lysate was split into two 50-ml tubes and centrifuged (15 min, 2,000 g, 4°C). The supernatant was carefully removed, and the pellet was resuspended on ice in 6 ml PBS/5 μ g/ml Cam. Subsequently, the 6 ml suspension was homogenized in 2 ml fractions with a ball homogenizer (Isobiotec) using an 8 μ m exclusion limit. Finally, the bacterial suspensions were transferred into FACS tubes and sorted with a FACSaria III (BD Biosciences). After FACS, the sorted bacterial populations were centrifuged (10,000 g, 20 min, 4°C), and the supernatant was carefully removed leaving approximately 200 μ l. The residual liquid was transferred in a 1.5-ml Eppendorf tube and centrifuged again (10,000 g, 20 min, 4°C). The supernatant was carefully removed leaving approximately 20 μ l, which was frozen at -80°C .

Alternatively, freshly sorted P_{flaA} -GFP-positive and P_{flaA} -GFP-negative *L. pneumophila* populations were subjected to replication assays and killing curves. To this end, *A. castellanii* amoebae were infected (MOI 5, 24 h), Amp (100 μ g/ml) was added to remove extracellular bacteria, and after an additional 18 h (in total 42 h of infection), the cells were homogenized at RT in the absence of protease inhibitor. After sorting of the bacteria, the tubes were centrifuged (2,000 g, 15 min), and the supernatant was carefully removed leaving 500 μ l. The pellet was resuspended and transferred into a 1.5-ml Eppendorf tube. The bacterial suspension was then used to infect (MOI 5, 2 h) 4×10^5 *A. castellanii* per well (grown overnight) in 24-well plates. After 2 h, the infected amoebae were washed and further incubated at 25°C for the time indicated. For the replication assays, the infected amoebae were lysed (24, 96 h), appropriate homogenate dilutions were plated on CYE plates, and CFU were determined. For the bi-phasic killing curves, the infected amoebae were treated with ofloxacin (30 μ g/ml). Finally, to assess bacterial viability, the sorted bacteria were directly plated on CYE plates.

Imaging flow cytometry

For imaging flow cytometry, amoebae were infected with *L. pneumophila* (MOI 5), and lysis and fixation was performed as outlined above for flow cytometry. After the last step, the bacteria were resuspended in 100 μ l PBS in a 1.5-ml Eppendorf tube. Using an Amnis ImageStream MK II (Luminex), (i) the bacteria in focus were gated using gradient RMS in the bright field channel, (ii) single bacteria were gated by plotting the area versus the aspect ratio in

the bright field channel, and (iii) single bacteria with different levels of the GFP fluorescence were gated by plotting the intensity of the GFP channel versus the intensity of the mCherry channel. After the gates were defined, 10,000 events per sample were acquired. Using the IDEAS 6.2 software, the gating of the bacterial population was repeated, and on a scatter plot depicting the fluorescence intensity in the green versus the red channel, multiple areas with increasing green fluorescence were selected to view their signal. Imaging flow cytometry was used to check the quality of sorting of the P_{flaA} -GFP-positive and P_{flaA} -GFP-negative subpopulations.

Electron microscopy

For EM, *A. castellanii* were infected (MOI 5, 2 h) with *L. pneumophila*, washed, and further incubated up to 48 h at 25°C. The supernatant, including highly infected cells, was collected and centrifuged (150 g, 5 min, 24°C). The cell pellet was aspirated into a cellulose capillary tube, immersed in 1-hexadecene, cut into pieces of 3–4 mm length, transferred into the 150 μ m well of a 6 mm aluminum specimen carrier, and sandwiched with a flat 6 mm aluminum specimen carrier wetted with 1-hexadecene. Samples were immediately frozen using an EM HPM 100 high-pressure freezing machine (Leica Microsystems, Vienna, Austria) without using alcohol as synchronization medium.

Freeze-substitution was carried out in water-free acetone containing 1% OsO_4 for 8 h at -90°C , 7 h at -60°C , 5 h at -30°C , and 2 h at 0°C , with transition gradients of 30°C per hour. Samples were rinsed twice with water-free acetone, block-stained with 1% uranyl acetate in acetone (stock solution: 20% in methanol) for 2 h at 4°C , rinsed twice with water-free acetone, and embedded in epon/ araldite: 66% in acetone overnight at 4°C , 100% for 1 h at RT, and polymerized at 60°C for 28 h. Ultrathin sections (50 nm) were post-stained with Reynolds lead citrate and imaged in a Talos 120 transmission electron microscope (TEM, Thermo Fisher Scientific, Eindhoven, The Netherlands) at 120 kV acceleration voltage, equipped with a bottom-mounted Ceta camera using the Maps software.

For immunogold-labeling on Tokuyasu sections, infected *A. castellanii* were centrifuged (40 g, 10 min), the supernatant was removed, and fixative solution (2% formaldehyde, 0.1% glutaraldehyde in 0.1 M cacodylate buffer, pH 7.35) was added (60 min, RT). The fixed amoebae were rinsed twice with cells collecting buffer (0.5% BSA in $1\times$ immuno-EM buffer; $10\times$ immuno-EM buffer: 0.15 M sodium phosphate buffer, 1.54 M NaCl) and centrifuged (14,000 g, 3 min). The supernatant was removed, and ca. 150 μ l of the cell pellet was carefully mixed with 800 μ l pre-warmed 12% gelatin in 0.1 M sodium phosphate buffer (5 min, 42°C). After centrifugation (14,000 g, 5 min), the polymerization of the pellet in gelatin occurred on ice (30 min). The cells in the gelatin block were cut into pieces $< 1 \text{ mm}^3$ on ice in cold 0.02 M sodium phosphate buffer containing 2.3 M sucrose. The pieces were infiltrated with 2.3 M sucrose in 0.02 M sodium phosphate buffer (16 h, 4°C) and placed in a fresh Eppendorf tube containing 2.3 M sucrose in 0.02 M sodium phosphate buffer. The specimens were stored at -20°C , or mounted on a cryo-pin, and frozen and stored in liquid N_2 .

For cryo-sectioning, a Leica cryo-ultramicrotome UC6 FC6 was used. The specimens on cryo-pins were mounted to the microtome arm in the cryo-chamber of the cryo-ultramicrotome set at -70°C and trimmed with a diamond cryo trim 45 knife at -70°C . 110-nm

ultrathin sections were cut at -110 to -120°C with a cryo-immuno 35° diamond knife. The sections were picked with a wired loop containing a droplet of pickup solution and transferred to a grid (50 mesh, nickel, formvar and carbon-coated, and glow discharged). Sections were stored at 4°C until further processing.

For immuno-labeling, the grids were washed with two drops of immuno-EM buffer (2×10 min on ice, and 2×20 min RT). The grids were left for at least 20 min on a drop of melted 2% gelatin type B in H_2O at 37°C on a heating plate in a petri dish and washed again with two drops of immuno-EM buffer. The washed grids were incubated in a drop of phosphate-buffered gelatin (PBG^+ ; 0.5% BSA, 0.2% gelatin type B in immuno-EM buffer) for 5 min and in a drop of primary antibody (mouse anti-GFP, 1:20 in PBG^+) for 60 min at RT. The grids were then washed with a drop of PBG^+ (6×2 min) and incubated with a drop of PBG^+ (5 min) and a secondary antibody (goat anti-mouse 12 nm gold, 1:20 in PBG^+) for 60 min on RT. The grids were again washed with a drop of PBG^+ (4×2 min) and a drop of immuno-EM buffer (3×1 min). The grids were subsequently incubated on a drop of 0.1% glutaraldehyde in immuno-EM buffer (5 min), washed in H_2O (6×1 min), and incubated on a drop of uranyl acetate/methylcellulose staining solution (0.3% uranyl acetate, 1.8% methylcellulose in H_2O) on ice for 5 min. Finally, the grids were removed with a self-made wired loop, and the supernatant was aspirated with filter paper and let dry over ice for 5–7 min. The grids were put in a grid box and investigated by TEM.

Quantification and statistical analysis

Statistical significance was determined using a two-tailed Student *t*-test on the means of at least three independent experiments. Probability values of less than 0.05, 0.01, and 0.001 are represented in the figures with *, **, or ***, respectively.

Data availability

All data are available in the main text or the supplementary material and provided as source data files. The mass spectrometry proteomics data have been deposited to the ProteomeXchange Consortium via the PRIDE partner repository with the dataset identifier PXD023787 (<https://doi.org/10.6019/PXD023787>).

Expanded View for this article is available online.

Acknowledgements

Research in the laboratory of H.H. was supported by the Swiss National Science Foundation (SNF; 31003A_175557, 310030_200706). N. P. was the recipient of an SNF Ambizione fellowship (PZ00P3_161492, PZ00P3_185529). The funders had no role in study design, data collection and analysis, decision to publish, or preparation of the manuscript. Open Access Funding provided by Universitat Zurich.

Author contributions

Conceived the study and raised the funds: HH and NP. Designed the experiments: BS, HH, and NP. Performed the experiments: BS, UL, AKat, SN, SV, SB, RH, AKae, AW, and NP. Analyzed the data: BS, UL, AKae, AW, HH, and NP. Contributed reagents/materials/analysis tools: UZ, AF, and AS. Wrote the manuscript: BS, HH, and NP. All authors read, amended, and approved the final manuscript.

Conflict of interest

The authors declare that they have no conflict of interest.

References

- Ackermann M (2015) A functional perspective on phenotypic heterogeneity in microorganisms. *Nat Rev Microbiol* 13: 497–508
- Ahrné E, Molzahn L, Glatter T, Schmidt A (2013) Critical assessment of proteome-wide label-free absolute abundance estimation strategies. *Proteomics* 13: 2567–2578
- Ahrné E, Glatter T, Vigano C, Schubert C, Nigg EA, Schmidt A (2016) Evaluation and improvement of quantification accuracy in isobaric mass tag-based protein quantification experiments. *J Proteome Res* 15: 2537–2547
- Albert-Weissenberger C, Sahr T, Sismeiro O, Hacker J, Heuner K, Buchrieser C (2010) Control of flagellar gene regulation in *Legionella pneumophila* and its relation to growth phase. *J Bacteriol* 192: 446–455
- Amer A, Franchi L, Kanneganti T-D, Body-Malapel M, Özören N, Brady G, Meshinchi S, Jagirdar R, Gewirtz A, Akira S et al (2006) Regulation of *Legionella* phagosome maturation and infection through flagellin and host IpaF. *J Biol Chem* 281: 35217–35223
- Appelt S, Heuner K (2017) The flagellar regulon of *Legionella* - a review. *Front Cell Infect Microbiol* 7: 454
- Arnoldini M, Vizcarra IA, Pena-Miller R, Stocker N, Diard M, Vogel V, Beardmore RE, Hardt WD, Ackermann M (2014) Bistable expression of virulence genes in *Salmonella* leads to the formation of an antibiotic-tolerant subpopulation. *PLoS Biol* 12: e1001928
- Asrat S, de Jesus DA, Hempstead AD, Ramabhadran V, Isberg RR (2014) Bacterial pathogen manipulation of host membrane trafficking. *Ann Rev Cell Dev Biol* 30: 79–109
- Aurass P, Schlegel M, Metwally O, Harding CR, Schroeder GN, Frankel G, Flieger A (2013) The *Legionella pneumophila* Dot/Icm-secreted effector PlcC/CegC1 together with PlcA and PlcB promotes virulence and belongs to a novel zinc metallophospholipase C family present in bacteria and fungi. *J Biol Chem* 288: 11080–11092
- Aurass P, Gerlach T, Becher D, Voigt B, Karste S, Bernhardt J, Riedel K, Hecker M, Flieger A (2016) Life stage-specific proteomes of *Legionella pneumophila* reveal a highly differential abundance of virulence-associated Dot/Icm effectors. *Mol Cell Proteomics* 15: 177–200
- Balaban NQ, Merrin J, Chait R, Kowalik L, Leibler S (2004) Bacterial persistence as a phenotypic switch. *Science* 305: 1622–1625
- Belyi Y, Jank T, Aktories K (2013) Cytotoxic glucosyltransferases of *Legionella pneumophila*. *Curr Top Microbiol Immunol* 376: 211–226
- Boamah DK, Zhou G, Ensminger AW, O'Connor TJ (2017) From many hosts, one accidental pathogen: the diverse protozoan hosts of *Legionella*. *Front Cell Infect Microbiol* 7: 477
- Brauner A, Fridman O, Gefen O, Balaban NQ (2016) Distinguishing between resistance, tolerance and persistence to antibiotic treatment. *Nat Rev Microbiol* 14: 320–330
- Brüggemann H, Hagman A, Jules M, Sismeiro O, Dillies M-A, Gouyette C, Kunst F, Steinert M, Heuner K, Coppee J-Y et al (2006) Virulence strategies for infecting phagocytes deduced from the *in vivo* transcriptional program of *Legionella pneumophila*. *Cell Microbiol* 8: 1228–1240
- Burton NA, Schurmann N, Casse O, Steeb AK, Claudi B, Zankl J, Schmidt A, Bumann D (2014) Disparate impact of oxidative host defenses determines the fate of *Salmonella* during systemic infection in mice. *Cell Host Microbe* 15: 72–83
- Campbell-Valois FX, Schnupf P, Nigro G, Sachse M, Sansonetti PJ, Parsot C (2014) A fluorescent reporter reveals on/off regulation of the *Shigella* type III secretion apparatus during entry and cell-to-cell spread. *Cell Host Microbe* 15: 177–189
- Carcamo-Oyarce G, Lumjiaktase P, Kümmerli R, Eberl L (2015) Quorum sensing triggers the stochastic escape of individual cells from *Pseudomonas putida* biofilms. *Nat Commun* 6: 5945
- Cirillo JD, Falkow S, Tompkins LS (1994) Growth of *Legionella pneumophila* in *Acanthamoeba castellanii* enhances invasion. *Infect Immun* 62: 3254–3261
- Claudi B, Sprote P, Chirkova A, Personnic N, Zankl J, Schurmann N, Schmidt A, Bumann D (2014) Phenotypic variation of *Salmonella* in host tissues delays eradication by antimicrobial chemotherapy. *Cell* 158: 722–733
- Conlon BP, Rowe SE, Gandt AB, Nuxoll AS, Donegan NP, Zalis EA, Clair G, Adkins JN, Cheung AL, Lewis K (2016) Persister formation in *Staphylococcus aureus* is associated with ATP depletion. *Nat Microbiol* 1: 16051
- Creasey EA, Isberg RR (2012) The protein SdhA maintains the integrity of the *Legionella*-containing vacuole. *Proc Natl Acad Sci USA* 109: 3481–3486
- Dalebroux ZD, Yagi BF, Sahr T, Buchrieser C, Swanson MS (2010) Distinct roles of ppGpp and DksA in *Legionella pneumophila* differentiation. *Mol Microbiol* 76: 200–219
- Davis KM, Mohammadi S, Isberg RR (2015) Community behavior and spatial regulation within a bacterial microcolony in deep tissue sites serves to protect against host attack. *Cell Host Microbe* 17: 21–31
- Diard M, Garcia V, Maier L, Remus-Emsermann MN, Regoes RR, Ackermann M, Hardt WD (2013) Stabilization of cooperative virulence by the expression of an avirulent phenotype. *Nature* 494: 353–356
- Faulkner G, Garduno RA (2002) Ultrastructural analysis of differentiation in *Legionella pneumophila*. *J Bacteriol* 184: 7025–7041
- de Felipe KS, Pampou S, Jovanovic OS, Pericone CD, Ye SF, Kalachikov S, Shuman HA (2005) Evidence for acquisition of *Legionella* type IV secretion substrates via interdomain horizontal gene transfer. *J Bacteriol* 187: 7716–7726
- de Felipe KS, Glover RT, Charpentier X, Anderson OR, Reyes M, Pericone CD, Shuman HA (2008) *Legionella* eukaryotic-like type IV substrates interfere with organelle trafficking. *PLoS Pathog* 4: e1000117
- Finsel I, Hilbi H (2015) Formation of a pathogen vacuole according to *Legionella pneumophila*: how to kill one bird with many stones. *Cell Microbiol* 17: 935–950
- Glatter T, Ludwig C, Ahrné E, Aebersold R, Heck AJ, Schmidt A (2012) Large-scale quantitative assessment of different in-solution protein digestion protocols reveals superior cleavage efficiency of tandem Lys-C/trypsin proteolysis over trypsin digestion. *J Proteome Res* 11: 5145–5156
- Grimbergen AJ, Siebring J, Solopova A, Kuipers OP (2015) Microbial bet-hedging: the power of being different. *Curr Opin Microbiol* 25: 67–72
- Hammer BK, Swanson MS (1999) Co-ordination of *Legionella pneumophila* virulence with entry into stationary phase by ppGpp. *Mol Microbiol* 33: 721–731
- Harms A, Maisonneuve E, Gerdes K (2016) Mechanisms of bacterial persistence during stress and antibiotic exposure. *Science* 354: aaf4268
- Heidman M, Chen EJ, Moy MY, Isberg RR (2009) Large-scale identification of *Legionella pneumophila* Dot/Icm substrates that modulate host cell vesicle trafficking pathways. *Cell Microbiol* 11: 230–248
- Hélaine S, Thompson JA, Watson KG, Liu M, Boyle C, Holden DW (2010) Dynamics of intracellular bacterial replication at the single cell level. *Proc Natl Acad Sci USA* 107: 3746–3751
- Hélaine S, Cheverson AM, Watson KG, Faure LM, Matthews SA, Holden DW (2014) Internalization of *Salmonella* by macrophages induces formation of nonreplicating persisters. *Science* 343: 204–208

- Hilbi H, Hoffmann C, Harrison CF (2011) *Legionella* spp. outdoors: colonization, communication and persistence. *Environ Microbiol Rep* 3: 286–296
- Hochstrasser R, Hilbi H (2017) Intra-species and inter-kingdom signaling of *Legionella pneumophila*. *Front Microbiol* 8: 79
- Hochstrasser R, Kessler A, Sahr T, Simon S, Schell U, Gomez-Valero L, Buchrieser C, Hilbi H (2019) The pleiotropic *Legionella* transcription factor LvbR links the Lqs and c-di-GMP regulatory networks to control biofilm architecture and virulence. *Environ Microbiol* 21: 1035–1053
- Hochstrasser R, Hilbi H (2020) *Legionella* quorum sensing meets cyclic-di-GMP signaling. *Curr Opin Microbiol* 55: 9–16
- Hochstrasser R, Hutter CA, Arnold FM, Bärlocher K, Seeger MA, Hilbi H (2020) The structure of the *Legionella* response regulator LqsR reveals amino acids critical for phosphorylation and dimerization. *Mol Microbiol* 113: 1070–1084
- Hoffmann C, Harrison CF, Hilbi H (2014) The natural alternative: protozoa as cellular models for *Legionella* infection. *Cell Microbiol* 16: 15–26
- Hovel-Miner G, Pampou S, Faucher SP, Clarke M, Morozova I, Morozov P, Russo JJ, Shuman HA, Kalachikov S (2009) SigmaS controls multiple pathways associated with intracellular multiplication of *Legionella pneumophila*. *J Bacteriol* 191: 2461–2473
- Hurtado-Guerrero R, Zusman T, Pathak S, Ibrahim AF, Shepherd S, Prescott A, Segal G, van Aalten DM (2010) Molecular mechanism of elongation factor 1A inhibition by a *Legionella pneumophila* glycosyltransferase. *Biochem J* 426: 281–292
- Inaba JI, Xu K, Kovalev N, Ramanathan H, Roy CR, Lindenbach BD, Nagy PD (2019) Screening *Legionella* effectors for antiviral effects reveals Rab1 GTPase as a proviral factor coopted for tombusvirus replication. *Proc Natl Acad Sci USA* 116: 21739–21747
- Jules M, Buchrieser C (2007) *Legionella pneumophila* adaptation to intracellular life and the host response: clues from genomics and transcriptomics. *FEBS Lett* 581: 2829–2838
- Kessler A, Schell U, Sahr T, Tiaden A, Harrison C, Buchrieser C, Hilbi H (2013) The *Legionella pneumophila* orphan sensor kinase LqsT regulates competence and pathogen-host interactions as a component of the LAI-1 circuit. *Environ Microbiol* 15: 646–662
- Kofoed EM, Vance RE (2011) Innate immune recognition of bacterial ligands by NAIPs determines inflammasome specificity. *Nature* 477: 592–595
- Koliwer-Brandl H, Knobloch P, Barisch C, Welin A, Hanna N, Soldati T, Hilbi H (2019) Distinct *Mycobacterium marinum* phosphatases determine pathogen vacuole phosphoinositide pattern, phagosome maturation, and escape to the cytosol. *Cell Microbiol* 21: e13008
- Kortebi M, Milohanic E, Mitchell G, Pechoux C, Prévost MC, Cossart P, Bierne H (2017) *Listeria monocytogenes* switches from dissemination to persistence by adopting a vacuolar lifestyle in epithelial cells. *PLoS Pathog* 13: e1006734
- Kulasekara BR, Kamischke C, Kulasekara HD, Christen M, Wiggins PA, Miller SI (2013) c-di-GMP heterogeneity is generated by the chemotaxis machinery to regulate flagellar motility. *eLife* 2: e01402
- Lang C, Hiller M, Flieger A (2017) Disulfide loop cleavage of *Legionella pneumophila* PlaA boosts lysophospholipase A activity. *Sci Rep* 7: 16313
- Laventie BJ, Sangermani M, Estermann F, Manfredi P, Planes R, Hug I, Jaeger T, Meunier E, Broz P, Jenal U (2019) A surface-induced asymmetric program promotes tissue colonization by *Pseudomonas aeruginosa*. *Cell Host Microbe* 25: 140–152
- Lightfield KL, Persson J, Brubaker SW, Witte CE, von Moltke J, Dunipace EA, Henry T, Sun Y-H, Cado D, Dietrich WF et al (2008) Critical function for Naip5 in inflammasome activation by a conserved carboxy-terminal domain of flagellin. *Nat Immunol* 9: 1171–1178
- Luo ZQ, Isberg RR (2004) Multiple substrates of the *Legionella pneumophila* Dot/Icm system identified by interbacterial protein transfer. *Proc Natl Acad Sci USA* 101: 841–846
- Manina G, Dhar N, McKinney JD (2015) Stress and host immunity amplify *Mycobacterium tuberculosis* phenotypic heterogeneity and induce nongrowing metabolically active forms. *Cell Host Microbe* 17: 32–46
- Mascarenhas DP, Zamboni DS (2017) Inflammasome biology taught by *Legionella pneumophila*. *J Leukoc Biol* 101: 841–849
- Moldoveanu AL, Rycroft JA, Hélaine S (2021) Impact of bacterial persisters on their host. *Curr Opin Microbiol* 59: 65–71
- Molmeret M, Alli OA, Radulic M, Susa M, Doric M, Kwaik YA (2002a) The C-terminus of IcmT is essential for pore formation and for intracellular trafficking of *Legionella pneumophila* within *Acanthamoeba polyphaga*. *Mol Microbiol* 43: 1139–1150
- Molmeret M, Alli OA, Zink S, Flieger A, Cianciotto NP, Kwaik YA (2002b) *icmT* is essential for pore formation-mediated egress of *Legionella pneumophila* from mammalian and protozoan cells. *Infect Immun* 70: 69–78
- Molofsky AB, Swanson MS (2003) *Legionella pneumophila* CsrA is a pivotal repressor of transmission traits and activator of replication. *Mol Microbiol* 50: 445–461
- Molofsky AB, Swanson MS (2004) Differentiate to thrive: lessons from the *Legionella pneumophila* life cycle. *Mol Microbiol* 53: 29–40
- Molofsky AB, Byrne BG, Whitfield NN, Madigan CA, Fuse ET, Tateda K, Swanson MS (2006) Cytosolic recognition of flagellin by mouse macrophages restricts *Legionella pneumophila* infection. *J Exp Med* 203: 1093–1104
- Mondino S, Schmidt S, Rolando M, Escoll P, Gomez-Valero L, Buchrieser C (2020) Legionnaires' disease: state of the art knowledge of pathogenesis mechanisms of *Legionella*. *Ann Rev Pathol* 15: 439–466
- Nagai H, Kagan JC, Zhu X, Kahn RA, Roy CR (2002) A bacterial guanine nucleotide exchange factor activates ARF on *Legionella* phagosomes. *Science* 295: 679–682
- Newton HJ, Ang DK, van Driel IR, Hartland EL (2010) Molecular pathogenesis of infections caused by *Legionella pneumophila*. *Clin Microbiol Rev* 23: 274–298
- Pereira MS, Marques GG, Dellama JE, Zamboni DS (2011a) The Nlr4 inflammasome contributes to restriction of pulmonary infection by flagellated *Legionella* spp. that trigger pyroptosis. *Front Microbiol* 2: 33
- Pereira MS, Morgantetti GF, Massis LM, Horta CV, Hori JI, Zamboni DS (2011b) Activation of NLRC4 by flagellated bacteria triggers caspase-1-dependent and -independent responses to restrict *Legionella pneumophila* replication in macrophages and *in vivo*. *J Immunol* 187: 6447–6455
- Personnic N, Bärlocher K, Finsel I, Hilbi H (2016) Subversion of retrograde trafficking by translocated pathogen effectors. *Trends Microbiol* 24: 450–462
- Personnic N, Striednig B, Hilbi H (2018) *Legionella* quorum sensing and its role in pathogen-host interactions. *Curr Opin Microbiol* 41: 29–35
- Personnic N, Striednig B, Hilbi H (2019a) Single cell analysis of *Legionella* and *Legionella*-infected *Acanthamoeba* by agarose embedment. *Methods Mol Biol* 1921: 191–204
- Personnic N, Striednig B, Lezan E, Manske C, Welin A, Schmidt A, Hilbi H (2019b) Quorum sensing modulates the formation of virulent *Legionella* persisters within infected cells. *Nat Commun* 10: 5216
- Personnic N, Striednig B, Hilbi H (2021) Quorum sensing controls persistence, resuscitation, and virulence of *Legionella* subpopulations in biofilms. *ISME J* 15: 196–210

- Qiu J, Luo ZQ (2017) *Legionella* and *Coxiella* effectors: strength in diversity and activity. *Nat Rev Microbiol* 15: 591–605
- Ragaz C, Pietsch H, Urwyler S, Tiaden A, Weber SS, Hilbi H (2008) The *Legionella pneumophila* phosphatidylinositol-4-phosphate-binding type IV substrate SidC recruits endoplasmic reticulum vesicles to a replication-permissive vacuole. *Cell Microbiol* 10: 2416–2433
- Ren T, Zamboni DS, Roy CR, Dietrich WF, Vance RE (2006) Flagellin-deficient *Legionella* mutants evade caspase-1- and Naip5-mediated macrophage immunity. *PLoS Pathog* 2: e18
- Sahr T, Rusniok C, Impens F, Oliva G, Sismeiro O, Coppee JY, Buchrieser C (2017) The *Legionella pneumophila* genome evolved to accommodate multiple regulatory mechanisms controlled by the CsrA-system. *PLoS Genet* 13: e1006629
- Schell U, Kessler A, Hilbi H (2014) Phosphorylation signalling through the *Legionella* quorum sensing histidine kinases LqsS and LqsT converges on the response regulator LqsR. *Mol Microbiol* 92: 1039–1055
- Schell U, Simon S, Hilbi H (2016a) Inflammasome recognition and regulation of the *Legionella* flagellum. *Curr Top Microbiol Immunol* 397: 161–181
- Schell U, Simon S, Sahr T, Hager D, Albers MF, Kessler A, Fahrnbauer F, Trauner D, Hedberg C, Buchrieser C et al (2016b) The α -hydroxyketone LAI-1 regulates motility, Lqs-dependent phosphorylation signalling and gene expression of *Legionella pneumophila*. *Mol Microbiol* 99: 778–793
- Schröter L, Dersch P (2019) Phenotypic diversification of microbial pathogens - cooperating and preparing for the future. *J Mol Biol* 431: 4645–4655
- Schulz T, Rydzewski K, Schunder E, Holland G, Bannert N, Heuner K (2012) FliA expression analysis and influence of the regulatory proteins RpoN, FleQ and FliA on virulence and *in vivo* fitness in *Legionella pneumophila*. *Arch Microbiol* 194: 977–989
- Sherwood RK, Roy CR (2016) Autophagy evasion and endoplasmic reticulum subversion: the Yin and Yang of *Legionella* intracellular infection. *Ann Rev Microbiol* 70: 413–433
- Silveira TN, Zamboni DS (2010) Pore formation triggered by *Legionella* spp. is an Nlr4 inflammasome-dependent host cell response that precedes pyroptosis. *Infect Immun* 78: 1403–1413
- Simon S, Hilbi H (2015) Subversion of cell-autonomous immunity and cell migration by *Legionella pneumophila* effectors. *Front Immunol* 6: 447
- Simon S, Schell U, Heuer N, Hager D, Albers MF, Matthias J, Fahrnbauer F, Trauner D, Eichinger L, Hedberg C et al (2015) Inter-kingdom signaling by the *Legionella* quorum sensing molecule LAI-1 modulates cell migration through an IQGAP1-Cdc42-ARHGEF9-dependent pathway. *PLoS Pathog* 11: e1005307
- Spirig T, Tiaden A, Kiefer P, Buchrieser C, Vorholt JA, Hilbi H (2008) The *Legionella* autoinducer synthase LqsA produces an α -hydroxyketone signaling molecule. *J Biol Chem* 283: 18113–18123
- Steiner B, Weber S, Hilbi H (2018) Formation of the *Legionella*-containing vacuole: phosphoinositide conversion, GTPase modulation and ER dynamics. *Int J Med Microbiol* 308: 49–57
- Swart AL, Harrison CF, Eichinger L, Steinert M, Hilbi H (2018) *Acanthamoeba* and *Dictyostelium* as cellular models for *Legionella* infection. *Front Cell Infect Microbiol* 8: 61
- Tiaden A, Spirig T, Weber SS, Brüggemann H, Bosshard R, Buchrieser C, Hilbi H (2007) The *Legionella pneumophila* response regulator LqsR promotes host cell interactions as an element of the virulence regulatory network controlled by RpoS and LetA. *Cell Microbiol* 9: 2903–2920
- Tiaden A, Spirig T, Carranza P, Brüggemann H, Riedel K, Eberl L, Buchrieser C, Hilbi H (2008) Synergistic contribution of the *Legionella pneumophila* lqs genes to pathogen-host interactions. *J Bacteriol* 190: 7532–7547
- Tiaden A, Spirig T, Hilbi H (2010a) Bacterial gene regulation by α -hydroxyketone signaling. *Trends Microbiol* 18: 288–297
- Tiaden A, Spirig T, Sahr T, Wälti MA, Boucke K, Buchrieser C, Hilbi H (2010b) The autoinducer synthase LqsA and putative sensor kinase LqsS regulate phagocyte interactions, extracellular filaments and a genomic island of *Legionella pneumophila*. *Environ Microbiol* 12: 1243–1259
- van Vliet S, Dal Co A, Winkler AR, Spriewald S, Stecher B, Ackermann M (2018) Spatially correlated gene expression in bacterial groups: the role of lineage history, spatial gradients, and cell-cell interactions. *Cell Syst* 6: 496–507
- Weber SS, Ragaz C, Reus K, Nyfeler Y, Hilbi H (2006) *Legionella pneumophila* exploits PI(4)P to anchor secreted effector proteins to the replicative vacuole. *PLoS Pathog* 2: e46
- Weber SS, Joller N, Küntzel AB, Spörri R, Tchang VS, Scandella E, Rösl C, Ludewig B, Hilbi H, Oxenius A (2012) Identification of protective B cell antigens of *Legionella pneumophila*. *J Immunol* 189: 841–849
- Weber S, Wagner M, Hilbi H (2014) Live-cell imaging of phosphoinositide dynamics and membrane architecture during *Legionella* infection. *MBio* 5: e00839-13
- Zamboni DS, Kobayashi KS, Kohlsdorf T, Ogura Y, Long EM, Vance RE, Kuida K, Mariathasan S, Dixit VM, Flavell RA et al (2006) The Birc1e cytosolic pattern-recognition receptor contributes to the detection and control of *Legionella pneumophila* infection. *Nat Immunol* 7: 318–325



License: This is an open access article under the terms of the Creative Commons Attribution-NonCommercial-NoDerivs License, which permits use and distribution in any medium, provided the original work is properly cited, the use is non-commercial and no modifications or adaptations are made.